

AD-757 332

DEEP OCEAN OPTICAL MEASUREMENT (DOOM)
REPORT: BAHAMA CHANNELS AND NORTH-
WESTERN ATLANTIC OCEAN

Donald E. Matlack

Naval Ordnance Laboratory
White Oak, Maryland

20 November 1972

DISTRIBUTED BY:

NTIS

National Technical Information Service
U. S. DEPARTMENT OF COMMERCE
5285 Port Royal Road, Springfield Va. 22151

AD 757332

NOLTR 72-284

DEEP OCEAN OPTICAL MEASUREMENT (DOOM)
REPORT; BAHAMA CHANNELS AND NORTH-
WESTERN ATLANTIC OCEAN

By
Donald E. Matlack

20 NOVEMBER 1972

DDC
RECEIVED
MAR 21 1973
REGULATED
B

NOL

NAVAL ORDNANCE LABORATORY, WHITE OAK, SILVER SPRING, MARYLAND

Reproduced by
NATIONAL TECHNICAL
INFORMATION SERVICE
U S Department of Commerce
Springfield VA 22151

APPROVED FOR PUBLIC RELEASE;
DISTRIBUTION UNLIMITED

Best Available Copy

NOLTR 72-284

UNCLASSIFIED

Security Classification

DOCUMENT CONTROL DATA - R & D

(Security classification of title, body of abstract and indexing annotation must be entered when the overall report is classified)

1. ORIGINATING ACTIVITY (Corporate author) Commander Naval Ordnance Laboratory White Oak, Silver Spring, Maryland 20910		2a. REPORT SECURITY CLASSIFICATION UNCLASSIFIED	
		2b. GROUP	
3. REPORT TITLE DEEP OCEAN OPTICAL MEASUREMENT (DOOM) REPORT; BAHAMA CHANNELS AND NORTHWESTERN ATLANTIC OCEAN			
4. DESCRIPTIVE NOTES (Type of report and inclusive dates) Interim Report			
5. AUTHOR(S) (First name, middle initial, last name) Donald E. Matlack			
6. REPORT DATE 20 November 1972		7a. TOTAL NO. OF PAGES 81	7b. NO. OF REFS 4
8a. CONTRACT OR GRANT NO.		9a. ORIGINATOR'S REPORT NUMBER(S) NOLTR 72-284	
b. PROJECT NO. Task ORD-03C-001-201-22		9b. OTHER REPORT NO(S) (Any other numbers that may be assigned this report)	
c.			
d.			
10. DISTRIBUTION STATEMENT Approved for public release; distribution unlimited			
11. SUPPLEMENTARY NOTES		12. SPONSORING MILITARY ACTIVITY Naval Ordnance Systems Command Washington, D. C.	
13. ABSTRACT In situ optical attenuation data obtained during Deep Ocean Optical Measurement (DOOM) program cruises D and E in 1969 are presented. Locales of operation were for Cruise D the Florida Straits and the Providence channels of the Bahama Islands and for Cruise E the western Atlantic from a coastal area off the Virginia Capes to the waters of the Sargasso Sea 300 nautical miles east of the Bahamas. Optical data presented are surface to bottom measurements of spectral attenuation coefficients at visible wavelengths in the transmission window interval and the volume scattering function at a wavelength of 436 nanometers. Subsequent measurement cruises are briefly discussed and DOOM program progress is updated.			

I

CONTENTS

	Page
I. INTRODUCTION.	1
II. CRUISE D NARRATIVE.	2
III. CRUISE D DATA	4
IV. CRUISE E NARRATIVE.	7
V. CRUISE E DATA PRESENTATION.	10
VI. CONCLUSION.	15
REFERENCES.	16
APPENDIX.	A-1

TABLES

I. VITAL STATISTICS OF CRUISE D
II. ATTENUATION SPECTRA FROM CRUISE D
III. VITAL STATISTICS OF CRUISE E
IV. ATTENUATION SPECTRA FROM CRUISE E
V. VOLUME SCATTERING FUNCTIONS FROM CRUISE E
VI. TOTAL ATTENUATION AND VOLUME SCATTERING COEFFICIENTS FOR SELECTED DEPTHS FROM CRUISE E

ILLUSTRATIONS

Figure	Title
1	DOOM Stations in the Northwestern Atlantic Ocean and Mediterranean Sea
2	Track Chart of DOOM Cruise D
3	Optical Attenuation and Temperature Profiles of Drop D-1
4	Optical Attenuation and Temperature Profiles of Drop D-2
5	Optical Attenuation and Temperature Profiles of Drop D-3
6	Optical Attenuation and Temperature Profiles of Drop D-4
7	Optical Attenuation and Temperature Profiles of Drop D-5A
8	Optical Attenuation and Temperature Profiles of Drop D-5B
9	Optical Attenuation Spectra of Drop D-2 at Selected Depths
10	Optical Attenuation Spectra of Drop D-5A at Selected Depths
11	Track Chart of DOOM Cruise E
12	Optical Attenuation and Temperature Profiles of Drop E-1
13	Optical Attenuation and Temperature Profiles of Drop E-3
14	Optical Attenuation and Temperature Profiles of Drop E-4
15	Optical Attenuation and Temperature Profiles of Drop E-5
16	Optical Attenuation Profiles of Bottom Waters of Drop E-5
17	Optical Attenuation and Temperature Profiles of Drop E-6
18	Comparative Attenuation Spectra from Three Cruise E Drops
19	Optical Attenuation Spectra of Drop E-4 at Selected Depths
20	Volume Scattering Functions at Selected Depths for Drop E-3
21	Volume Scattering Function as Computed by Morrisson from Argus Island Measurements
22	$R(\theta)$ vs Scattering Angle for Selected Scattering Data of Morrissons from Argus Island during August 1966
A1	Corrected Figure 17 of NOLTR 70-165
A2	Corrected Figure 22 of NOLTR 70-165
A3	Schematic of the Exterior Optics of the Attenuation Measurement Section

I. INTRODUCTION

The objective of the Deep Ocean Optical Measurement (DOOM) program is to measure quantitatively those optical characteristics of the ocean which restrict the underwater transmission of light. Specific parameters to be investigated are the attenuation coefficients in the near ultraviolet and visible spectral regions, the volume scattering coefficient at a wavelength of 436 nanometers, and the background illumination in the transmission window around 470 nanometers. To accomplish this task, DOOM instrumentation has been developed which will procure in situ the desired optical data to any depth in the ocean. DOOM equipments and operations are fully described in reference 1.

Data are collected during measurement cruises aboard research vessels of the AGOR class operated by the Naval Oceanographic Office for east coast Navy laboratories. From December 1967 to June of 1972, nine cruises were completed in various areas of the western North Atlantic Ocean and the Mediterranean and Caribbean seas. Instrument drops were made at a total of 73 different stations as shown in Figure 1. Equipment difficulties primarily in the early stages of the measurements have limited the quantity of useful data obtained at perhaps 30 percent of these stations. However, the total data amassed to date is considered an adequate statistical sampling of these ocean areas and thus completes the collection phase of the DOOM program in Atlantic waters.

Although a great deal of raw data has been partially processed, much still requires further reduction and preparation prior to publication. Due to the numerous requests that have been received for DOOM data, this interim report of fully processed data is being released. Thorough analysis and interpretation of results will not be attempted until more of the finished data becomes available. This report presents the complete results of optical measurements during two voyages, cruises D and E, in the western North Atlantic and the Bahama Islands. DOOM program progress will be updated with brief discussions on measurement cruises completed since the last technical report NOLTR 70-165(1). Some errors in this previous report which have been brought to our attention, will be corrected in the appendix and some topics will be elaborated upon which may possibly have been treated too tersely. Successful use of dielectric mirrors for the external optics in the water path will be discussed.

II. CRUISE D NARRATIVE

The fourth DOOM measurement cruise, D, departed Key West, Florida aboard the USNS GILLIS, T-AGOR-4 on the afternoon of 27 March 1969, tracked as shown in Figure 2 through the Florida Straits and Bahama channels, and returned to port at Port Everglades, Florida on 2 April 1969. Mechanical failure of ship's equipment and high seas in the Straits of Florida prevented operations until the early morning of 29 March when the somewhat calmer waters of the Northwest Providence Channel were reached. During the succeeding four nights five additional measurements drops were completed at the stations shown in Figure 2. Pertinent data on each drop are presented in Table 1.

Prior to cruise D the complete DOOM system was tested underwater at the Undersea Weapons Tank facility at the Naval Ordnance Laboratory. The exterior stepper motor of the scattering section flooded during these trials, suffering irreparable damage. A replacement motor could not be obtained in time for sailing, so the scattering measurement was necessarily restricted to a fixed angle. Since this was the first time a DOOM scattering measurement was attempted at sea, we didn't have a good feel for expected signal amplitudes, so the minimum forward scattering angle of six degrees was selected in order to insure signals of measurable levels. The grating monochromator of the attenuation measurement section was programmed to scan a spectral range from 408 to 577 nanometers in 18 approximately equal steps. Time required for a complete spectrum was one minute. Signal processing electronics had been rebuilt prior to the cruise in order to eliminate non-linear thermal effects which had degraded system performance on earlier cruises.

Drop D-1 was made in the lee of Grand Bahama Island in order to avoid the large swell which had been buffeting the ship in the Straits of Florida. Since this was the first in situ test of the reworked electronics, the drop was programmed to determine if the hysteresis effect of the α signal as a function of lowering direction had been corrected. After starting on deck the package was gradually lowered to a depth of 1000 meters which was in cold water well below the thermocline and then raised to the surface while still operating. A close approach to the bottom was not attempted for fear that the time consuming approach operation might not permit ample time for continuous measurements during the ascent to the surface. During pre-drop check out the 40 V power line supplying the mercury arc lamp was inadvertently shorted to ground. Damage to the system was restricted to the 40 volt circuitry, which was completely burned out. The rest of the instruments functioned normally, so we proceeded with the drop minus the scattering measurement.

Examination of the drop D-1 raw data revealed that our new electronics had indeed solved the hysteresis problem since the up signals retraced those recorded on the way down. In succeeding drops we would concentrate on obtaining data during the descent and in positioning the package close to the bottom. The mercury lamp circuitry was replaced and performed satisfactorily during the remainder of the cruise.

Drop D-2 was made on the evening of 29 March in the middle of the Northwest Providence channel in slightly shallower water than of the preceding morning. Prevailing fair weather and calm seas permitted placement of the package on the bottom at a depth of 923 meters. By the following evening the ship had steamed further east along the channel into deeper water, about 1920 meters, for drop D-3. Sea and wind had picked up which resulted in appreciable drift and pitch of the ship during the operation. As the package approached the bottom, the depth had decreased to 1887 meters and was still coming up. Due to the uncertainty in bottom topography and the aggravated surface condition, the package was stopped for its safety some 37 meters from the bottom.

The next station was scheduled in the ocean area east of the islands at a depth in excess of 4500 meters. As we departed the islands through the Northeast Providence channel, we encountered a rather rough sea with high swell which was forecast to worsen as we proceeded out to sea. It was decided to stop after crossing the 2100 fathom (3840 meter) contour which could be reached in a reasonably short time due to the sharp fall off of the bottom topography east of the Bahamas. The drop was completed again taking care not to impact the package on the bottom.

Two stations were planned for the next night prior to entering port. Both were scheduled in the Florida Straits off Port Everglades; the first near the axis of the Gulf Stream and the second as close to shore as the ship could safely maneuver. The relative shallowness of the water and the proximity of the stations would allow time to complete both drops during the same night. Drop D-5A was conducted in the early evening of 1 April in mid-channel where the package was placed within six meters of the sea floor, a depth of 326 meters. The wind on this evening was coming off the ocean from the east and tended to push the ship towards the shore. This resultant drift prevented both a really close-in coastal measurement and a near bottom package approach since the ship throughout the drop continually drifted into shallower water towards the beach.

III. CRUISE D DATA

Data from the six measurement drops of cruise D are presented in Figures 3 through 10 and in Table II. Attenuation and temperature are plotted as a function of depth for the respective drops in Figures 2 through 8; spectral information are presented in Figures 9 and 10 and in Table II. Attenuation parameters generally plotted versus depth are the attenuation coefficients at two wavelengths, 483 nm in the transmission window and 432 nm nearly coincident with the scattering wavelength at 436 nm, and the volume scattering function at six degrees forward scattering angle. An exception is drop D-1 where only α is presented at wavelengths of 408 nm and 483 nm. Figures 9 and 10 illustrate for drops D-2 and D-5A respectively the spectral variation of attenuation at various depths throughout the water column. Attenuation spectra for all drops are presented at selected depths in Table II. A tabular form for the presentation of spectral data is considered appropriate since numerous plots of spectra result in confusion of data points and curves and would thus tend to make individual spectra difficult to distinguish.

As previously mentioned, the scattering section was inoperative during drop D-1 and the primary objective was to test the electronics of the spectral attenuation measurement. Although these electronics proved stable, a problem did arise concerning the quantitative calibration of the spectral measurement. This calibration consists of a spectral measurement run in an essentially zero attenuation medium, in our case air, prior to each drop. It is quite obvious that external mirrors and windows must be absolutely clean. Since the DOOM package is secured to the deck on the fan tail, calibrations are necessarily run in the open exposed to the elements. During inclement weather it is virtually impossible to guarantee that the exterior optics remain clean or perhaps more important free of moisture. An erroneous calibration was recorded under these conditions prior to drop D-1. When this occurs a calibration spectra from an adjoining drop may be quite validly used since the system response remains reasonably stable during this time interval. In this case, however, there was no usable adjacent calibrations, since D-1 was the first of the cruise and prior to D-2 amplifier gain was increased in order to produce larger signal deflections. Once the DOOM package enters the water, mirrors are wetted and hence rinsed of contaminants, so good qualitative data may be produced although a quantitative error exists. Since amplifier gain remained constant and the up and down signals coincided quite nicely, it is felt that qualitatively, D-1 data is valid. Minimum values of α , from the clearest portion of the water column, have been adjusted to coincide with comparable minimum values obtained during drop D-2. No spectra are presented however because the calibration error and the gain change introduce spectral distortions which cannot be accurately corrected.

Attenuation profiles of drops D-1, D-2, D-3 and D-4, all measured in the tropical waters in or near the Bahamas, exhibit a number of common features. Values of α in the surface waters range from 0.12 to 0.15 m^{-1} at the 483 nm wavelength. Higher values of α are associated with nepheloid layers occurring within 50 meters of the surface. In these layers of intense scattering, α increases rapidly to a peak as in drop D-2 at 35 meters, where α is seen to increase by about 0.013 m^{-1} to a peak value of 0.165 m^{-1} . That this increase is associated with scattering is verified by the scattering function profile which increases in an identical manner.

Below the surface layer, attenuation gradually drops to a minimum of from 0.03 to 0.04 m^{-1} at depths between 400 and 500 meters. In all cases the descent is not smooth, but exhibits varying degrees of structure. This structure may take the form of distinct peaks as in drop D-3 where multiple peaks appear at depths of 30, 60 and 180 meters; or it may appear as inflections in the slope of the profile as in drop D-1 where a plateau occurs at around 100 meters. Generally, structure in the attenuation profile correspond to changes in the temperature profile with peaks appearing nominally in regions of strong temperature gradients.

After passing through the region of minimum attenuation between 400 and 600 meters, α increases slightly by about 0.01 m^{-1} , and then remains essentially constant to the bottom. Drop D-2 does show a slight increase in turbidity near the ocean floor.

Drops D-5A and D-5B were made in the Florida Straits where current and temperature structure are somewhat more complicated. Surface waters for drop D-5A in the Gulf Stream were slightly warmer than those of the Bahamas and were isothermal to a depth of around 60 meters where a steep thermocline produced a prominent attenuation spike. Values of α were comparable to those previously measured in the Bahamas. Attenuation decreases rapidly following the peak and varies somewhat irregularly to the bottom. Minimum attenuation occurs at a depth of 230 meters which corresponds to the bottom of a minor temperature inversion. Drop D-5B was made closer to shore in the counter current which is adjacent to and slightly cooler than the Gulf Stream waters. Profiles show two distinct attenuation peaks at depths of 45 and 135 meters and a minimum α at about 165 meters, almost 30 meters from the bottom. The peak α at 483 nm of 0.18 m^{-1} was the highest of the cruise. Minimum α 's in the Straits were between 0.04 and 0.05 m^{-1} which is slightly higher than those found in the Bahama channels. The scattering function similarly is higher; clear water values range from 0.015 and 0.025 $\text{ster}^{-1}\text{m}^{-1}$ as compared with α 's of about 0.015 $\text{ster}^{-1}\text{m}^{-1}$ for the Bahama waters.

Spectra at selected depths throughout the water column are presented for drops D-2 and D-5A in Figures 9 and 10 respectively. The major difference we observe between spectra is that of amplitude rather than the gradual trends that lead to subtle variation in spectral shape. For instance in drop D-2, the total change in α

between spectra is about 0.14 m^{-1} , which for the transmission window wavelength of 480 nanometers is over 80 percent of the maximum value of 0.17 m^{-1} . Common spectral features are the window at 480 nm and a broad but rather weak absorption band at 520 nm. A close examination reveals that attenuation at the shorter wavelengths varies over a greater range than for the longer wavelengths. The maximum change in α of 0.14 m^{-1} between the clearest and most turbid waters occurs at the shortest wavelength, 410 nm. In the window region from 450 to 500 nm difference drops to 0.13 m^{-1} and continues to decrease with increasing wavelength to 0.10 m^{-1} at 577 nm. Even the clearer water below 200 meters exhibit a somewhat smaller attenuation change at the longer wavelengths. The effect of this spectral dependence is to more nearly equalize attenuation on each side of the window in the higher turbidity waters. The character of the window is consequently changed from a rather broad interval between 450 and 490 nanometers for the clear water case to a narrow interval for the turbid water case at a slightly longer wavelength, 480 nanometers.

Spectra of drop D-5A vary both in amplitude and shape in much the same manner as drop D-2. The flattening effect due to the enhanced short wavelength attenuation in the more turbid water is illustrated by the top curve, 63 meter depth, where α varies by only 0.035 m^{-1} over the spectral measurement interval. Another feature of the 63 meter curve that should be noted is the apparent downward shift of the three data points below 440 nm. Discontinuous data points may also be observed in other curves at one or more wavelengths. Such errors are attributed to the continuous motion of the package in the inhomogeneous ocean. Although the package is sometimes stopped at specific depths for short periods during lowering, the majority of measurements are recorded while moving in a gradual descent. Since a spectrum is scanned but once a minute, the measurement occurs over a small depth increment. If the water is vertically structured then a significant spectral change may occur during the time span of a single spectrum. Although obvious distortions are excluded from the data reduction process, spectra recorded in strata of peak attenuation where α is subject to rapid change may include such discontinuities. The three short wavelength data points at 63 meters may reflect such an error. Individual wavelengths which deviate from the spectral curve can be attributed to localized impurities, perhaps a large plankton, within the measurement path.

Selected spectra from all the six drops are presented in Table II. When studying these spectra, remember that the ocean is not a homogeneous medium and hence discontinuities may appear in the spectral curves.

IV. CRUISE E NARRATIVE

The fifth DOOM voyage, cruise E, departed Norfolk, Virginia on 17 October 1969 aboard the USNS LYNCH for two weeks at sea in the western North Atlantic. Six measurement drops were completed as shown on the cruise track, Figure 11, before debarking on 29 October at Port Everglades, Florida. Eleven stations were scheduled on the nights of 17 to 27 October; the remaining two days were required for transit back to port. Inclement weather prevented operations at five of the eleven stations. A recorder malfunction resulted in the total loss of data from drop E-2. Relevant data on the five successful drops are presented in Table III.

Modifications were made to both the attenuation and scattering measurement sections in preparation for cruise E. The scan rate of the grating monochrometer was increased from one to four scans per minute in order to decrease the thickness of the water layer over which a complete spectrum is recorded. The wavelength interval of the spectral measurement was shifted by 22 nanometers towards the shorter wavelengths, producing a new spectral interval from 386 to 555 nanometers. This resulted in a more central position of the transmission window and more nearly equal attenuation at both wavelength extremes. A new stepper motor was installed for the scattering section thus permitting measurement of the volume scattering function through angles from 6 to 92°.

Station E-1 was located on the shelf in shallow, 30 meter, water about 40 miles off the southern Virginia coastline. Previous DOOM measurements had been confined to clear "blue water" ocean areas, so for comparison a measurement in much more turbid coastal water was desired. The recently modified measurement sections performed quite nicely during this first drop.

Drops E-2 and E-3 were made further east, about 150 nautical miles from the Virginia Capes, in the waters of the Gulf Stream. XBT casts prior to the drops revealed the existence of several strong thermal inversions in a highly structured surface profile to a depth of about 140 meters. Consequently very slow lowering rates with stops within the inversion were planned while in the stratified surface layers. Unfortunately rather crude winch controls do not permit precise regulation of lowering operations. A desirable lowering rate in this case might be three meters per minute so that a complete spectrum would be recorded about every 1.5 meters and a scattering function every three meters. Surface waters would be sampled then in about an hour, leaving two hours to complete the descent to the bottom. Lowest speeds obtainable with this winch ranged between 10 and 15 meters per minute which regrettably limits the vertical accuracy of the attenuation data. As previously mentioned no data were obtained from drop E-2. Good spectral attenuation data were obtained in drop E-3 to the maximum package depth of 3065 meters, about 80 meters from the bottom. The scattering trace performed normally until a depth of about 2000 meters

where signal levels as a function of angle began to deviate from anticipated values. Large off-scale signals appeared at the minimum angular six degree position. Obviously the stepper mirror had lost synchronization and off-scale signals were caused by rotation of the source beam past the six degree stop until it was incident upon the receiver entrance window. Several explanations for the loss of synch were plausible: a failure or intermittent operation of the stepper drive circuitry, a loosening of the motor in its mount due to hydrostatic pressure, or binding of the motor shaft due again to increased pressure, or partial flooding of the underwater electrical connectors. Inspection of the system revealed that the motor was slightly out of position, so it was realigned and securely fastened. Drive circuitry and electrical continuity appeared normal. Perhaps then the failure must be attributed to the effect of large hydrostatic pressure upon the motor. During subsequent drops angular phasing was again lost at depths around 2000 meters. We concluded that insufficient torque was available to drive the motor at these depths and that redesign of the drive circuitry was required to obtain more driving force.

A station was lost due to inclement seas prior to drop E-4 on 22 October. This station, much farther south in the Sargasso sea was in deep water, 5120 meters, over the Hatteras abyssal plain. A maximum package depth of only 3000 meters was reached because the drop was programmed to proceed very slowly at the intermediate depths in order to ascertain when synch was lost by the scattering measurement section.

Rough seas again prevented operations until the night of 26 October when the weather abated somewhat. Seas were still higher than desirable, but since our cruise time was running out, the risks were considered justifiable. Drops E-5 and E-6 were made in deep water over the Hatteras plain at stations about 500 nautical miles east of the Florida coast. Close approaches to the bottom were accomplished for both drops. However, when the package surfaced from drop E-6 wires of the lifting bridle were snarled and a lifting eye on the top hemisphere of the instrument sphere was severely bent. Attempted straightening of the eye resulted in its shearing off which thus prevented opening the sphere and removal of data. Since this was the last scheduled station, we sailed for Port Everglades where the facilities of the NOL Test Facility at Fort Lauderdale could be employed for equipment repair. Subsequent inspection of equipment and examination of data revealed that at a depth of 625 meters the package was completely inverted. An optical filter holder which fitted over a lens mount and thus was held in position by both gravity and friction had slid off its mount. This could occur only if the instrument was tipped over and banged about. Spillage of battery electrolyte, snarling of supporting bridle wires, and abrasion of wires and hardware confirmed the inversion. The question then was, what caused it? Could the package have struck a sufficiently large submerged object, either natural or man-made at such a depth to tip it over? Or could a combination of operational factors such as rough seas, rather violent pitching of the ship,

and too fast a lowering rate allow sufficient slack to develop in the wire that it would pitch over? Initially, I supported the first contention, but now with additional experience at sea, I lean towards the latter explanation. Nevertheless, displacement of the filter ruined the α data for the remainder of drop E-6.

V. CRUISE E DATA PRESENTATION

Optical data will be presented in much the same manner as for cruise D. That is, attenuation data in the form of the scattering function at a particular angle and α at a fixed wavelength in the transmission window will be plotted as a function of depth. Next spectral α will be presented. Then scattering as a function of angle and calculations of the total volume scattering coefficient will be discussed.

Attenuation profiles are presented in Figures 12 through 17. Levels of attenuation in the coastal measurement, Figure 12 are about twice those observed for the most turbid "blue water" ocean measurements. Increased attenuation in the water layer at 28 meters is due to mixing of silt from the shallow bottom. Profiles of drop E-3, Figure 13, dramatically illustrate the rapid variation of attenuation within the steep temperature gradients of an inversion. The surface waters to a 200 meter depth, presented here with the depth scale expanded, include three inversions, two large ones at depths of 80 and 108 meters and a small one at 116 meters. The three prominent peaks in the profiles correspond with both slopes of the first inversion and the bottom of the second inversion. Broken lines indicate extreme turbidity where weak signal levels fell below the threshold sensitivity of the recording system. This kind of variation in attenuation perhaps should be expected in such a highly structured water column since the various strata are composed of waters from three different ocean areas. Water masses involved are the relatively clear waters of the Gulf Stream, the cooler more turbid coastal waters, and the extremely clear Sargasso Sea waters from the mid-Atlantic. Certainly each of these water types would possess somewhat different optical characteristics. The very large peaks however are attributed to planktonic layers within the thermal gradients. Once through the surface waters temperature continually decreases, α reaches a plateau at about 0.05 m^{-1} , and $\sigma(60)$ drops gradually to $0.013 \text{ m}^{-1} \text{ster}^{-1}$ until synch is lost at 1750 meters. A slight increase in α is observed near the bottom.

In drops E-4, E-5, and E-6 a different thermal structure than previously observed is present in the upper 1500 meters. Surface water is isothermal to an initial thermocline at 40 to 60 meter depths. Temperature falls rapidly in the roughly 150 meter thick thermocline from 24 to 16°C, then essentially levels off at a plateau temperature of 15 to 16°C between 200 and 600 meters, and then decreases rapidly again in a second thermocline to 5°C at 1000 meters. The profile then more or less levels out and slowly decreases with depth. As usual, high attenuation exists in the isothermal layer at the surface and a small peak appears at the first thermocline. Surface α 's of 0.07 to 0.09 m^{-1} are somewhat lower than previously measured in the Bahama waters. An exceptionally high clarity water is present at the base of the initial thermocline, which persists throughout the 15-16°C plateau

and partway down the second thermocline. This water, with α 's from 0.025 to 0.030 m^{-1} , is the clearest yet measured during the DOOM voyages. Below this clear region at the base of the second thermocline, a rather broad, yet modest peak centered at 1300 meters occurs in the α profile. α increases by about 0.015 m^{-1} . The scattering function, $\sigma(60^\circ)$, does not peak, but its rate of descent is essentially arrested as in drop E-4, Figure 14, where it levels off at 0.02 $\text{m}^{-1}\text{ster}^{-1}$. Below this secondary peak α levels off at around 0.03 m^{-1} until the influence of the bottom proximity is felt. During drop E-5 this effect on α began about 1000 meters from the ocean floor and increased quite dramatically as the bottom was approached. The general trend as seen in Figure 16 is a nearly exponential increase as the package closes with the bottom. The curve however is not smooth but possesses a number of structural features. Minima occur at several depths, the first a rather broad minimum near the base of the slope at 4400 meters and two sharper ones at 4800 and 4890 meter depths. The peak of the profile is not reached at the maximum package depth of 4930 meters, some 20 meters from the bottom but at 4910 meters another 20 meters higher. Maximum attenuation of the bottom waters, $\alpha = 0.12 \text{ m}^{-1}$, exceeded that of the surface layer. This general increase in turbidity near the bottom is attributed to turbulence produced by bottom currents. An explanation for the structure is not so evident. It has been postulated (2) that the turbidity peaks may be coincident with adjacent topographic heights and thus result from lateral transport of particulate material from such prominences.

The variety of different ocean water types sampled during cruise E represented the most turbid and the clearest waters encountered at that time during DOOM operations. Attenuation spectra varied significantly both in magnitude and shape as shown in Figures 18 and 19 and in Table IV. Spectra from three stations covering the complete turbidity range are presented in Figure 18. Two spectra from the murky coastal drop E-1 appear at the top of the figure. Severe attenuation prevailed throughout the spectral interval of the measurement but was especially strong at short wavelengths where low transmitted signal levels fell below the threshold sensitivity of the system. Four spectra of drop E-3, the Gulf Stream station, are presented, three from the layered surface waters and one from the clear intermediate water column. Attenuation spectra from the surface layers, though still fairly high in amplitude, fall well below the coastal water curves, and are quite variable in shape and amplitude. Coefficients at the shorter wavelengths are greatly reduced relative to the rest of the curve except in the inversion layer at 80 meters where the curve essentially parallels those of the coastal water. Perhaps then this inversion is a layer of low salinity coastal water which is mixing with the clear more saline warm waters of the Gulf Stream and Sargasso Sea. Below the surface strata the deeper water spectra are fairly uniform in shape. The bottom curve, from the clean intermediate water of drop E-5 is representative of the clearest water measured by DOOM. More surprising than the low α of 0.025 m^{-1} in the transmission

window, are the values of around 0.04 m^{-1} in the deep violet below 400 nanometers. The 4930 meter curve from drop E-5 is from the turbulent sediment laden waters near the bottom. Although much higher in amplitude, $\alpha = 0.107 \text{ m}^{-1}$, the spectral shape does not differ appreciably from the clearer waters except for slightly higher relative attenuation at the shorter wavelengths. The diverse spectra of Figure 18 lucidly illustrates the trend of the transmission window to shift the longer wavelength with increasing turbidity. Also illustrated is the marked increase of attenuation in the shorter blue-violet wavelengths relative to the longer green-yellow spectral interval.

Representative spectra of the clear waters prevailing in the Sargasso Sea during cruise E are presented in Figure 19 for drop E-4. The two spectra from the isothermal layer above the primary thermocline are quite unique. Relative attenuation at the shorter wavelengths is very low resulting in a shift of the center of the transmission window to around 440 nanometers. Spectral shapes of other depths are typical of relatively clear water where the window is centered close to 480 nanometers. Although the magnitudes of α 's at these short wavelengths were low relative to the rest of the spectrum, they were still substantially higher than comparable wavelengths of the deeper clear water spectra. This characteristic spectral curve for the isothermal surface water was observed at all three of the Sargasso sea stations.

During cruise E the in situ scattering measurement was made for the first time as a function of angle. The volume scattering function can therefore be presented at the various angles as in Figure 20 where data from drop E-3 is plotted at selected depths. A log-log scale is used because the ordinate term $\sigma(\theta)$ varies over several decades and because it is desirable to expand the angular term of the abscissa at the small forward angles since they make such a large contribution to the total scattering coefficient. The plotted data of Figure 20 produces a series of nearly parallel curves which tend to converge slightly at the larger angles. The first data point of each curve is at 6° , the minimum angle of the scattering measurement. The maximum angle plotted is determined by the level of the scattering signal which decreases both with increasing angle and increasing water clarity. The last data point is at the largest angle where the signal level still falls within the logarithmic range of the amplifier electronics. Maximum depth is dependent upon where the stepper mirror lost synchronization. Scattering functions for all the drops are presented in Table V.

The objective of the DOOM scattering measurement is to determine the total volume scattering coefficient, s . This can be accomplished by integrating the volume scattering function, $\sigma(\theta)$, over the entire angular interval from 0 to 180° . Unfortunately, our measurement in most cases extends only from 6° to 35° , so we must develop a technique for extrapolating to both the smaller and larger angular extremities. Our technique will be developed

from the works of Morrison (4,5), primarily from his data taken in the "blue water" ocean at Argus Island, a Texas Tower located 25 miles southwest of Bermuda. The values of α measured during August 1966 in these rather shallow waters, maximum depth was 55 meters, ranged from 0.20 to 0.09 m^{-1} which is representative of reasonably clear ocean water. If we look at a typical curve of $\sigma(\theta)$, Figure 21, the reason for using a log-log plot becomes quite obvious. Since values of the scattering function become quite large at the very small forward angles as θ approaches 0° , the log-log plot permits a more detailed examination of the data. It appears that the angular interval of the DOOM data makes only a minor contribution to the total integral. Morrison presents the term $R(\theta)$, which is defined by the equation

$$R(\theta) = \frac{\int_0^\theta \sigma(\theta) \sin \theta d\theta}{\int_0^\pi \sigma(\theta) \sin \theta d\theta} = \frac{2\pi \int_0^\theta \sigma(\theta) \sin \theta d\theta}{s}$$

$R(\theta)$ then is the cumulative ratio of the portion of the total scattering coefficient obtained by integration from 0° to the angle θ , divided by the total scattering coefficient. This quantity tells us what fraction of s is due to scattering at angles less than θ . The function $R(\theta)$ is presented in Figure 22 for Morrison's Argus Island measurements of August 1966. Data were recorded during four measurements periods at 12 depths equally spaced between surface and bottom. This curve represents the average $R(\theta)$ function calculated from 44 of the 48 individual measurements of the scattering function. The discarded curves, from near surface data during only two of the four measurement periods, differ significantly from the rest of the functions. The average fractional contribution to the total coefficient in the DOOM interval from 6° to 35° is 0.228. Standard deviation of this mean is 0.0175. Total s for the DOOM measurements are calculated by multiplying the reciprocal of this factor, 4.39, by the integral of the scattering function over the 6° to 35° interval. Values of α at 432 nm and of s at the 436 nm Hg line are presented at selected depths for the cruise E stations in Table VI. The general trend within each drop is for the fraction of the attenuation loss due to scattering to decrease with decreasing total attenuation. In the more turbid northern waters of drops E-1 and E-3, the primary attenuation process appears to be due to absorption since s is usually less than half of α . The exception is the 12 meter depth in the chaotic surface waters of drop E-3 where s at 0.176 m^{-1} is about 63 percent of the total. In the surface waters of the Sargasso Sea there is an obvious problem with coefficients since s exceeds or nearly equals α in drops E-4, E-5, and E-6. Since I have confidence in the measured value of α , I feel that the error exists in the method of calculating the total s from the DOOM angular measurement interval. The four $R(\theta)$ functions excluded from the average, differed in that a smaller fraction of the total s was contributed at the smaller forward

scattering angles. That is, a larger portion of the total s was in the DOOM interval, in one case close to 40 percent. A correction by this amount would tend to bring values of s into a more reasonable range. It must also be remembered that α 's at Bermuda were somewhat higher than for the DOOM data under discussion. What must be concluded, then, is that the shape of the $R(\theta)$ function is not really uniform even for reasonably clear ocean waters, and that to accurately measure s , the scattering function must be determined in the small angle region, less than 1° in the forward direction.

VI. CONCLUSION

Three measurement cruises (G, H and I), have been completed since the last DOOM report, NOLTR 70-165. Cruise G in February 1971 departed Jamaica, operated to the northwest in the Cayman Trough, through the Yacatan Straits, and along the northwest coast of Cuba, before terminating in Key West, Florida. Cruise H in April-May 1971 departed Norfolk, Virginia, tracked southeast to a station about 300 nautical miles east of Cape Hatteras, then tracked northeast to the Grand Banks, and entered port at Argentia, Newfoundland. Cruise I in March and April 1972 departed Athens, Greece, steamed west through the Mediterranean Sea, through the straits of Gibraltar, and entered the Atlantic port of Rota, Spain. The number of measurement drops for cruises G, H, and I respectively were 9, 12 and 13. Although flawless performance of the DOOM system was not always achieved, a large quantity of fine data was collected during the three cruises.

Data reduction and analysis of the DOOM measurements is unfortunately somewhat laborious and time consuming. Funding and manpower limitations necessarily restrict the rate and quantity of the output of processed data. Publication similarly has been retarded. The measurement phase of the Atlantic Ocean survey of the DOOM program has been tentatively completed, so that effort during the current fiscal year will be devoted to the processing and reporting of measurement results.

REFERENCES

1. Donald E. Matlack, "The Deep Ocean Optical Measurement (DOOM) Program", NOLTR 70-165, 18 January 1971
2. N. G. Jerlov, "Optical Oceanography", Elsevier Publishing Company, 1968
3. R. E. Morrison, "Experimental Studies on the Optical Properties of Sea Water", Journal Geophys. Res., 75, 612-628, 1970
4. R. E. Morrison, "Characteristics of the Optical Volume Scattering Function of Sea Water", J. Ocean. Soc. Japan, Vol. 26, No. 2, 101-107, 1970

TABLE I
VITAL STATISTICS OF CRUISE D

Drop #	Date	Time	Latitude North	Longitude West	Depth (m)	Maximum Package Depth (m)
D-1	3-29-69	0416	26° 30'	78° 11'	1161	1000
D-2	3-29-69	2145	26° 10'	78° 15.5'	923	923
D-3	3-30-69	2329	26° 04'	77° 45.5'	1887	1850
D-4	3-31-69	2045	25° 42'	77° 02'	3842	3790
D-5A	4-1-69	1911	26° 01'	79° 50'	326	320
D-5B	4-1-69	2325	26° 0.8.9'	80° 01.1'	219	198

TABLE II ATTENUATION SPECTRA FROM CRUISE D

Drop #	D-2	D-2	D-2	D-2	D-2	D-2	D-2	D-2	D-2	D-2
Depth (m)	7	32	103	209	398	597	720	886	923	
Wavelength λ (nm)	Spectral Attenuation Coefficient $a(\lambda)$ (m^{-1})									
408	.175	.191	.124	.079	.056	.058	.061	.066	.072	
419	.167	.183	.112	.070	.048	.047	.053	.058	.066	
432	.162	.176	.108	.067	.045	.043	.050	.053	.060	
443	.160	.175	.106	.066	.045	.040	.045	.045	.056	
454	.157	.173	.108	.066	.041	.038	.045	.048	.056	
465	.154	.170	.101	.063	.040	.037	.043	.045	.051	
473	.153	.169	.099	.064	.040	.037	.043	.045	.051	
483	.151	.167	.098	.061	.040	.037	.041	.045	.051	
491	.153	.172	.101	.066	.045	.040	.045	.048	.054	
500	.157	.175	.106	.070	.050	.045	.051	.051	.058	
508	.166	.183	.111	.079	.060	.054	.061	.063	.066	
519	.172	.188	.120	.089	.069	.066	.069	.072	.077	
528	.172	.188	.122	.092	.072	.069	.070	.076	.080	
537	.173	.189	.127	.095	.077	.072	.077	.080	.085	
546	.182	.193	.133	.103	.085	.080	.085	.089	.093	
557	.188	.198	.146	.112	.093	.089	.093	.098	.101	
568	.195	.204	.153	.118	.101	.099	.101	.108	.111	
577	.208	.214	.167	.131	.115	.114	.117	.122	.125	

TABLE II (Continued)

Drop #	D-3	D-3	D-3	D-3	D-3	D-3	D-3	D-3	D-3	D-3	D-3	D-3	D-3
Depth (m)	5	32	48	60	136	177	392	650	817	1200	1600	1850	
Wavelength λ (nm)	Spectral Attenuation Coefficient $\alpha(\lambda)$ (m^{-1})												
408	.169	.183	.157	.157	.085	.087	.051	.056	.064	.061	.060	.058	
419	.157	.170	.147	.147	.074	.077	.041	.048	.053	.051	.050	.048	
432	.154	.169	.143	.143	.070	.076	.038	.043	.048	.048	.045	.043	
443	.153	.164	.141	.143	.067	.076	.037	.038	.045	.043	.041	.040	
454	.153	.166	.141	.141	.069	.076	.035	.039	.045	.043	.041	.040	
465	.147	.159	.138	.138	.066	.074	.035	.037	.040	.041	.038	.037	
473	.147	.157	.138	.140	.066	.074	.036	.038	.041	.041	.038	.037	
483	.144	.154	.137	.137	.066	.072	.037	.037	.040	.040	.037	.037	
491	.146	.157	.140	.140	.069	.077	.040	.039	.045	.043	.043	.041	
500	.151	.160	.141	.143	.074	.080	.045	.045	.050	.048	.047	.045	
508	.157	.169	.151	.151	.083	.090	.056	.056	.060	.058	.056	.054	
519	.166	.178	.159	.160	.095	.099	.067	.066	.069	.068	.066	.064	
528	.167	.176	.160	.162	.096	.099	.069	.069	.072	.070	.069	.067	
537	.170	.182	.166	.166	.101	.105	.076	.074	.079	.077	.077	.076	
546	.175	.186	.170	.170	.108	.111	.082	.082	.087	.083	.082	.082	
557	.183	.195	.178	.178	.115	.117	.092	.090	.095	.093	.090	.090	
568	.189	.199	.186	.186	.125	.125	.099	.101	.098	.103	.101	.099	
577	.204	.212	.199	.201	.138	.140	.115	.114	.118	.115	.115	.115	

TABLE II (Continued)

Drop #	D5-A	D5-A	D5-A	D5-A	D5-A	D5-A	D5-A	D5-A	D5-A
Depth (m)	7	30	63	92	150	220	276	318	
Wavelength λ (nm)	Spectral Attenuation Coefficient $\alpha(\lambda)$ (m^{-1})								
408	.147	.153	.182	.115	.095	.067	.072	.072	.072
419	.143	.144	.180	.105	.085	.061	.064	.064	.063
432	.141	.143	.172	.096	.079	.056	.058	.058	.061
443	.140	.140	.180	.099	.072	.051	.054	.054	.056
454	.138	.141	.178	.090	.070	.048	.053	.053	.054
465	.133	.137	.176	.087	.066	.047	.048	.048	.051
473	.135	.137	.173	.087	.066	.048	.048	.048	.051
483	.131	.135	.175	.083	.064	.047	.047	.047	.050
491	.135	.137	.176	.089	.067	.050	.050	.050	.051
500	.140	.140	.180	.093	.074	.054	.054	.054	.056
508	.147	.147	.183	.101	.083	.064	.064	.064	.065
519	.157	.156	.184	.112	.093	.074	.074	.074	.074
528	.156	.156	.182	.112	.093	.076	.076	.076	.077
537	.160	.160	.185	.117	.099	.080	.080	.080	.082
546	.166	.167	.189	.122	.108	.090	.085	.085	.089
557	.170	.172	.194	.128	.114	.096	.096	.096	.096
568	.182	.182	.198	.138	.125	.108	.108	.108	.106
577	.195	.195	.210	.153	.138	.120	.120	.120	.120

TABLE I1 (Continued)

Drop #	D5-B	D5-B	D5-B	D5-B	D5-B	D5-B	D5-B	D5-B
Depth (m)	5	25	45	65	105	165	198	
Wavelength λ (nm)	Spectral Attenuation Coefficient $\alpha(\lambda)$ (m^{-1})							
408	.138	.166	.212	.156	.089	.070	.080	
419	.131	.160	.204	.147	.082	.064	.076	
432	.131	.156	.195	.141	.077	.061	.069	
443	.131	.154	.198	.138	.074	.056	.064	
454	.131	.156	.201	.137	.072	.054	.066	
465	.127	.153	.189	.131	.066	.050	.058	
473	.128	.151	.193	.130	.067	.051	.060	
483	.125	.147	.183	.128	.066	.048	.060	
491	.128	.156	.196	.131	.070	.053	.064	
500	.131	.162	.205	.137	.076	.060	.067	
508	.141	.170	.217	.144	.087	.066	.077	
519	.149	.178	.228	.153	.095	.077	.085	
528	.147	.178	.228	.157	.098	.077	.087	
537	.153	.183	.228	.160	.103	.085	.093	
546	.160	.189	.231	.167	.112	.093	.099	
557	.169	.196	.234	.172	.120	.101	.108	
568	.173	.204	.239	.178	.127	.111	.115	
577	.189	.217	.251	.193	.143	.125	.130	

TABLE III
VITAL STATISTICS OF CRUISE E

Drop #	Date	Time	Latitude North	Longitude West	Depth	Maximum Package Depth (m)
E-1	10-18-69	1920	36° 39.1'	75° 10.4'	28.5	28.5
E-2	10-19-69	1946	36° 34'	73° 22'	3054	3000
E-3	10-20-69	1926	36° 40'	73° 12'	3145	3065
E-4	10-22-69	2124	31° 28'	73° 14'	5121	3000
E-5	10-26-69	1818	28° 13.2'	71° 43.5'	4953	4930
E-6	10-27-69	1854	26° 44'	71° 41'	5150	5140

TABLE IV
ATTENUATION SPECTRA FROM CRUISE E

Drop #	E-1	E-2	E-1	E-1	E-1	E-3	E-3	E-3	E-3	E-3	E-3
Depth (m)	5	13.5	20	27	28	12	43	80	120	125	
Wavelength λ (nm)	Spectral Attenuation Coefficient (m^{-1})										
	$\alpha(\lambda)$										
386	-	-	-	-	-	-	.239	-	.124	.113	
398	-	-	-	-	-	.342	.220	-	.117	.108	
410	-	-	-	-	-	.318	.211	.334	.109	.101	
421	.459	.470	.449	.491	-	.300	.200	.305	.103	.096	
432	.437	.441	.418	.465	.476	.289	.188	.278	.095	.105	
443	.410	.414	.392	.446	.461	.276	.181	.249	.099	.101	
451	.395	.400	.378	.430	.451	.272	.176	.238	.105	.095	
461	.378	.386	.359	.421	.432	.264	.159	.222	.106	.086	
469	.368	.370	.351	.421	.432	.258	.150	.213	.101	.079	
478	.360	.367	.343	.410	.424	.256	.144	.203	.100	.074	
486	.356	.359	.340	.405	.413	.251	.134	.201	.100	.076	
497	.348	.349	.333	.402	.411	.254	.138	.198	.101	.078	
506	.351	.352	.332	.400	.421	.257	.143	.197	.109	.080	
515	.357	.360	.349	.408	.432	.265	.154	.204	.117	.095	
524	.359	.360	.341	.410	.440	.268	.159	.206	.122	.098	
535	.362	.367	.344	.416	-	.268	.162	.206	.124	.106	
546	.364	.372	.343	.416	-	.273	.173	.210	.131	.111	
555	.373	.383	.349	.421	-	.276	.182	.216	.138	.122	

TABLE IV (Continued)

Drop #	E-3	E-3	E-3	E-3	E-3	E-3	E-3	E-4	E-4	E-4	E-4	E-4
Depth (m)	280	560	840	2110	3065	10	40	68	88	100		
Wavelength λ (nm)	Spectral Attenuation Coefficient $\alpha(\lambda)$ (m^{-1})											
386	.095	.107	.086	.076	.101	.077	.080	.134	.104	.096		
398	.089	.090	.077	.071	.096	.071	.073	.127	.100	.088		
410	.086	.086	.073	.064	.087	.064	.068	.116	.088	.076		
421	.079	.080	.068	.060	.079	.066	.068	.112	.082	.074		
432	.074	.076	.066	.058	.077	.066	.066	.109	.080	.070		
443	.066	.070	.058	.052	.073	.066	.066	.103	.075	.066		
451	.068	.068	.057	.051	.068	.066	.066	.105	.073	.063		
461	.068	.066	.057	.051	.071	.068	.068	.101	.073	.063		
469	.065	.063	.055	.051	.058	.071	.070	.101	.075	.066		
478	.063	.064	.055	.051	.064	.070	.073	.099	.076	.065		
486	.063	.063	.057	.051	.068	.068	.072	.098	.075	.065		
497	.065	.064	.055	.053	.068	.074	.075	.099	.080	.066		
506	.071	.073	.063	.058	.074	.077	.080	.106	.085	.073		
515	.082	.080	.074	.070	.086	.090	.090	.112	.094	.084		
524	.087	.086	.079	.072	.090	.096	.100	.114	.098	.086		
535	.092	.094	.082	.080	.096	.101	.103	.119	.102	.092		
546	.096	.098	.092	.090	.103	.108	.111	.126	.107	.098		
555	.105	.106	.099	.096	.111	.115	.119	.133	.115	.106		

TABLE IV (Continued)

Drop #	E-4	E-4	E-4	E-4	E-4	E-4	E-4	E-4	E-4
Depth (m)	280	605	1200	1300	1400	1690	2840	3000	2260
Wavelength λ (nm)	Spectral Attenuation Coefficient $\alpha(\lambda)$ (m^{-1})								
386	.047	.044	.076	.070	.074	.064	.049	.048	.051
398	.038	.038	.066	.067	.063	.056	.045	.047	.041
410	.037	.033	.056	.054	.058	.046	.038	.040	.035
421	.035	.028	.056	.053	.052	.044	.035	.039	.033
432	.031	.028	.054	.051	.051	.044	.035	.034	.031
443	.030	.027	.046	.045	.042	.038	.028	.031	.025
451	.028	.024	.044	.043	.044	.035	.028	.029	.025
461	.027	.025	.042	.042	.040	.036	.027	.028	.022
469	.029	.028	.042	.043	.044	.038	.030	.031	.025
478	.029	.027	.042	.045	.044	.037	.028	.032	.027
486	.028	.025	.042	.043	.041	.037	.027	.031	.024
497	.030	.028	.044	.043	.042	.038	.029	.032	.028
506	.038	.038	.049	.051	.049	.043	.035	.039	.035
515	.052	.049	.060	.061	.060	.054	.049	.050	.045
524	.057	.057	.064	.069	.066	.062	.054	.056	.052
535	.064	.064	.073	.073	.073	.072	.064	.064	.060
546	.070	.066	.078	.082	.081	.074	.068	.072	.066
555	.079	.076	.089	.088	.087	.086	.078	.080	.070

TABLE IV (Continued)

Drop #	E-5	E-5	E-5	E-5	E-5	E-5	E-5	E-5	E-5	E-5	E-5
Depth (m)	10	90	410	690	1375	2040	3640	4660	4880	4930	
Wavelength λ (nm)	Spectral Attenuation Coefficient $\alpha(\lambda)$ (m ⁻¹)										
386	.086	.068	.038	.044	.063	.046	.060	.088	.136	-	
398	.074	.058	.031	.038	.060	.043	.051	.082	.131	.138	
410	.073	.058	.028	.035	.055	.040	.047	.076	.122	.131	
421	.074	.057	.030	.033	.051	.038	.044	.073	.119	.125	
432	.073	.051	.027	.028	.049	.031	.042	.070	.114	.121	
443	.070	.046	.022	.027	.043	.028	.035	.066	.108	.113	
451	.073	.047	.024	.025	.035	.028	.035	.063	.105	.109	
461	.071	.046	.022	.024	.038	.027	.033	.058	.105	.109	
469	.074	.049	.024	.024	.038	.027	.035	.060	.105	.108	
478	.073	.047	.024	.024	.041	.027	.033	.060	.104	.106	
486	.073	.053	.025	.022	.039	.025	.033	.058	.100	.108	
497	.078	.058	.030	.028	.043	.030	.038	.060	.105	.109	
506	.082	.062	.035	.033	.049	.038	.039	.068	.108	.111	
515	.098	.075	.049	.046	.060	.049	.057	.081	.125	.122	
524	.104	.076	.053	.051	.066	.052	.062	.084	.124	.128	
535	.107	.084	.060	.055	.071	.063	.068	.092	.131	.135	
546	.112	.089	.065	.068	.078	.068	.074	.097	.135	.141	
555	.122	.095	.074	.072	.087	.076	.081	.106	.143	.148	

TABLE IV (Continued)

Drop #	E-6	E-6	E-6	E-6	E-6	E-6	E-6	E-6	E-6
Depth (m)	7	40	80	100	160	300	620		
Wavelength λ (nm)	Spectral Attenuation Coefficient $\alpha(\lambda)$ (m^{-1})								
386	.080	.086	.111	.086	.060	.038	.042		
398	.076	.079	.095	.076	.055	.035	.039		
410	.077	.078	.090	.073	.051	.033	.036		
421	.077	.077	.089	.070	.049	.031	.036		
432	.077	.077	.090	.068	.049	.031	.035		
443	.074	.078	.086	.066	.042	.027	.030		
451	.077	.080	.084	.066	.041	.028	.030		
461	.077	.079	.084	.066	.038	.028	.030		
469	.079	.079	.084	.064	.042	.029	.030		
478	.079	.080	.082	.064	.040	.028	.030		
486	.079	.082	.086	.066	.041	.028	.031		
497	.084	.087	.089	.071	.047	.033	.035		
506	.090	.093	.093	.076	.052	.039	.039		
515	.106	.105	.103	.089	.064	.054	.054		
524	.109	.109	.112	.093	.068	.060	.058		
533	.112	.114	.112	.095	.077	.064	.064		
546	.119	.121	.119	.103	.080	.073	.070		
555	.127	.128	.127	.110	.090	.081	.080		

TABLE V
VOLUME SCATTERING FUNCTIONS FROM CRUISE E

Drop #	E-1	E-1	E-1	E-3	E-3	E-3	E-3	E-3	E-3
Depth (m)	5	13.5	20	28	12	52	70	80	96
θ (Degrees)					$\sigma(\theta)$ (m^{-1} ster $^{-1}$)				
6.0	.264	.253	.206	.259	.278	.109	.197	.159	.077
13.2	.065	.062	.052	.070	.082	.032	.052	.043	.022
20.4	.024	.024	.020	.030	.031	.012	.019	.018	.0093
27.6	.011	.010	.0095	.014	.014	.0057	.0089	.0082	.0044
34.8	.0062	.0064	.0059	.0074	.0076	.0031	.0057	.0054	.0030
49.2	.0034	.0031	.0029	.0043	.0039	-	-	-	-
Drop #	E-3	E-3	E-3	E-3	E-3	E-4	E-4	E-4	E-4
Depth (m)	108	125	280	820	1750	10	40	68	88
θ (Degrees)					$\sigma(\theta)$ (m^{-1} ster $^{-1}$)				
6.0	.112	.042	.032	.016	.012	.165	.165	.167	.133
13.2	.033	.013	.0090	.0050	.0042	.029	.031	.032	.024
20.4	.013	.0063	.0044	.0025	.0013	.012	.011	.013	.0094
27.6	.0069	.0035	.0025	-	-	.0055	.0051	.0058	.0040
31.8	.0043	.0022	.0020	-	-	.0031	.0030	.0031	.0025
49.2	-	-	-	-	-	-	-	-	-

TABLE V (Continued)

Drop #	E-4	E-4	E-4	E-4	E-4	E-4	E-4	E-4	E-4
Depth (m)	100	120	280	605	1200	1300	1500	1690	
θ (Degrees)	$\sigma(\theta)$ (m^{-1} ster $^{-1}$)								
6.0	.092	.064	.038	.030	.019	.019	.019	.022	
13.2	.017	.013	.0074	.0062	.0037	.0037	.0038	.0046	
20.4	.070	.0048	.0033	.0029	.0018	.0018	.0018	.0021	
27.6	.0033	.0025	.0020	.0017	-	-	-	-	
34.8	.0022	.0019	-	-	-	-	-	-	

3

Drop #	E-5	E-5	E-5	E-5	E-5	E-5	E-5	E-5	E-5
Depth (m)	10	60	90	120	160	270	550	830	1380
θ (Degrees)	$\sigma(\theta)$ (m^{-1} ster $^{-1}$)								
6.0	.143	.110	.060	.041	.036	.027	.025	.018	.016
13.2	.028	.023	.015	.0098	.0074	.0062	.0052	.0037	.0033
20.4	.011	.0089	.0061	.0041	.0041	.0028	.0024	.0018	.0016
27.6	.0045	.0036	.0026	.0020	.0017	.0016	.0014	.0011	.0011
34.8	.0026	.0020	.0016	.0015	.0013	.0013	.0013	-	-

TABLE V (Continued)

Drop #	E-6	E-b	E-6	E-6	E-6	E-6	E-6	E-6	E-6
Depth (m)	7	80	120	160	200	300	430	620	
θ (Degrees)	$\sigma(\theta)$ (m^{-1} ster $^{-1}$)								
6.0	.110	.114	.055	.034	.027	.023	.021	.017	
13.2	.030	.032	.016	.0090	.0074	.0064	.0061	.0048	
20.4	.012	.014	.0064	.0041	.0032	.0030	.0027	.0022	
27.6	.0054	.0060	.0029	.0021	.0019	.0017	.0018	.0015	
34.8	.0029	.0029	.0017	.0016	.0015	.0013	.0014	.0013	

TABLE VI

TOTAL ATTENUATION AND VOLUME SCATTERING COEFFICIENTS FOR
SELECTED DEPTHS FROM CRUISE E

Depth (m)	α (m^{-1})	s (m^{-1})
DROP E-1		
5	.437	.153
13.5	.441	.142
20	.418	.126
28	.491	.178
DROP E-3		
12	.281	.176
52	.160	.067
70	.298	.115
80	.272	.096
96	.229	.049
108	.305	.063
125	.105	.031
280	.078	.023
820	.064	.015
1750	.057	.010
DROP E-4		
10	.068	.075
40	.068	.075
68	.109	.075
88	.071	.057
100	.068	.043
120	.052	.030
280	.030	.022
605	.030	.015
1200	.054	.010
1300	.052	.010
1500	.044	.010
1690	.044	.012

TABLE VI (Continued)

Depth (m)	α (m^{-1})	s (m^{-1})
DROP E-5		
10	.074	.067
60	.082	.052
90	.053	.035
120	.041	.024
160	.033	.020
270	.027	.016
550	.028	.014
830	.036	.010
1090	.042	.009
1380	.047	.009
DROP E-6		
7	.078	.070
80	.090	.077
120	.068	.037
160	.049	.023
200	.038	.019
300	.031	.016
430	.033	.015
620	.035	.013

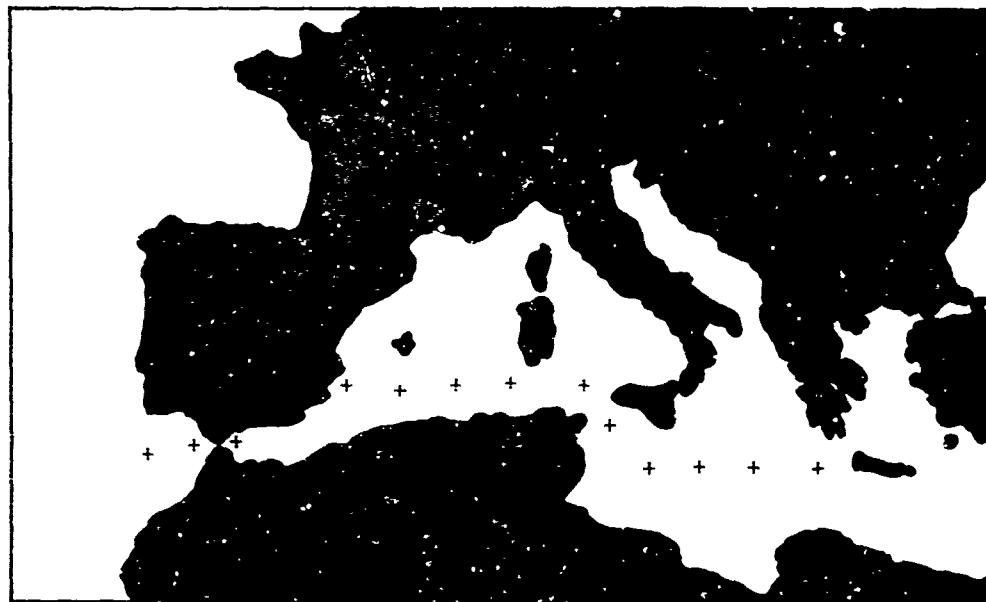
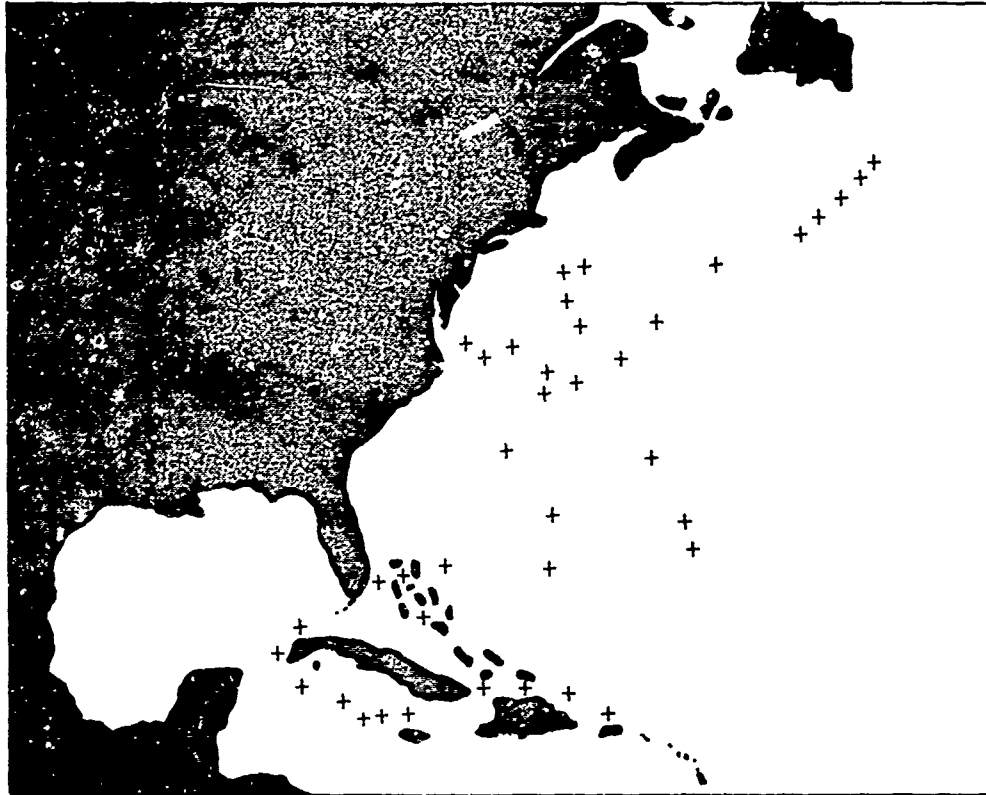


FIG. 1 DOOM STATIONS IN THE NORTHWESTERN ATLANTIC OCEAN AND MEDITERRANEAN SEA

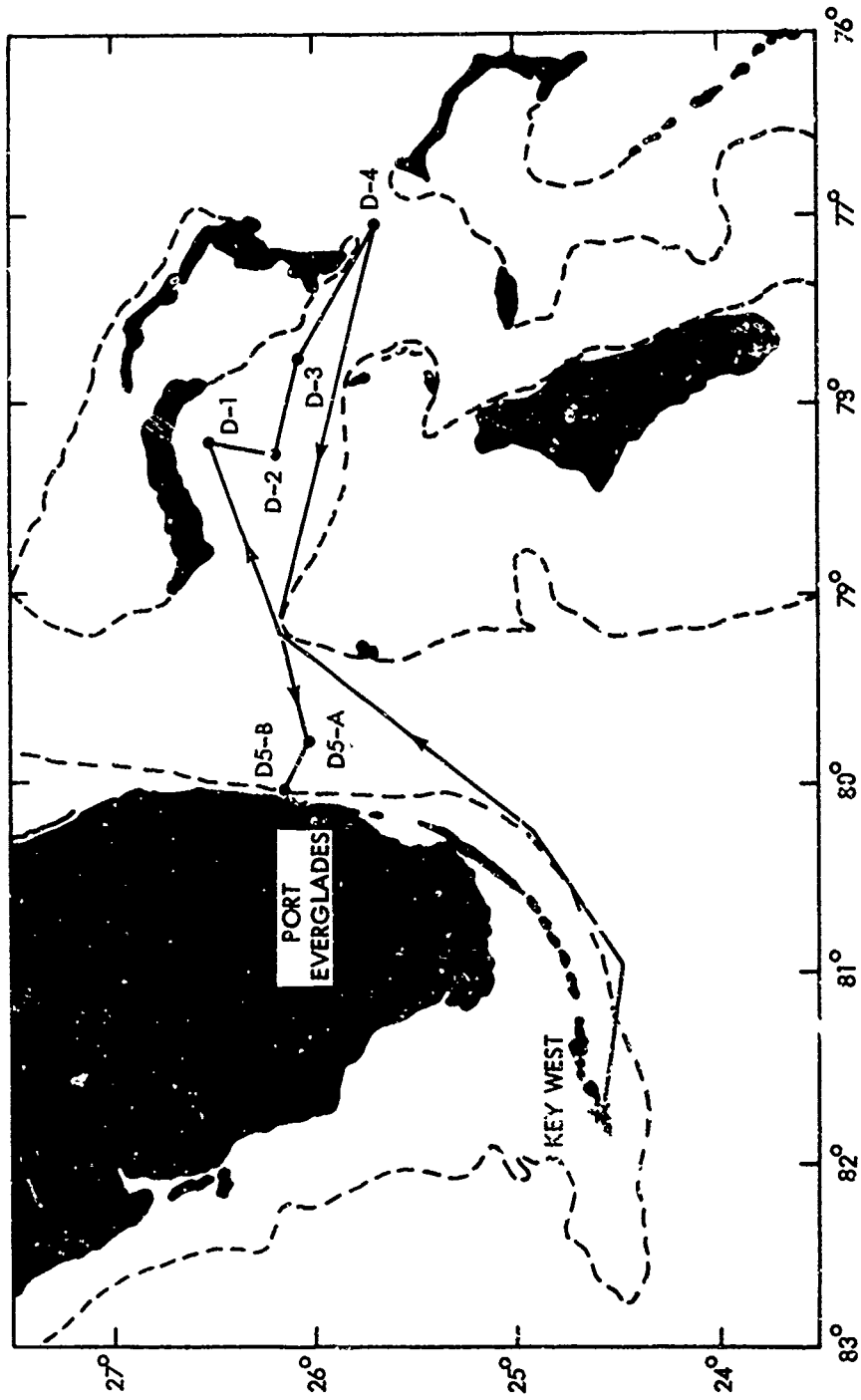


FIG. 2 TRACK CHART OF DOOM CRUISE D

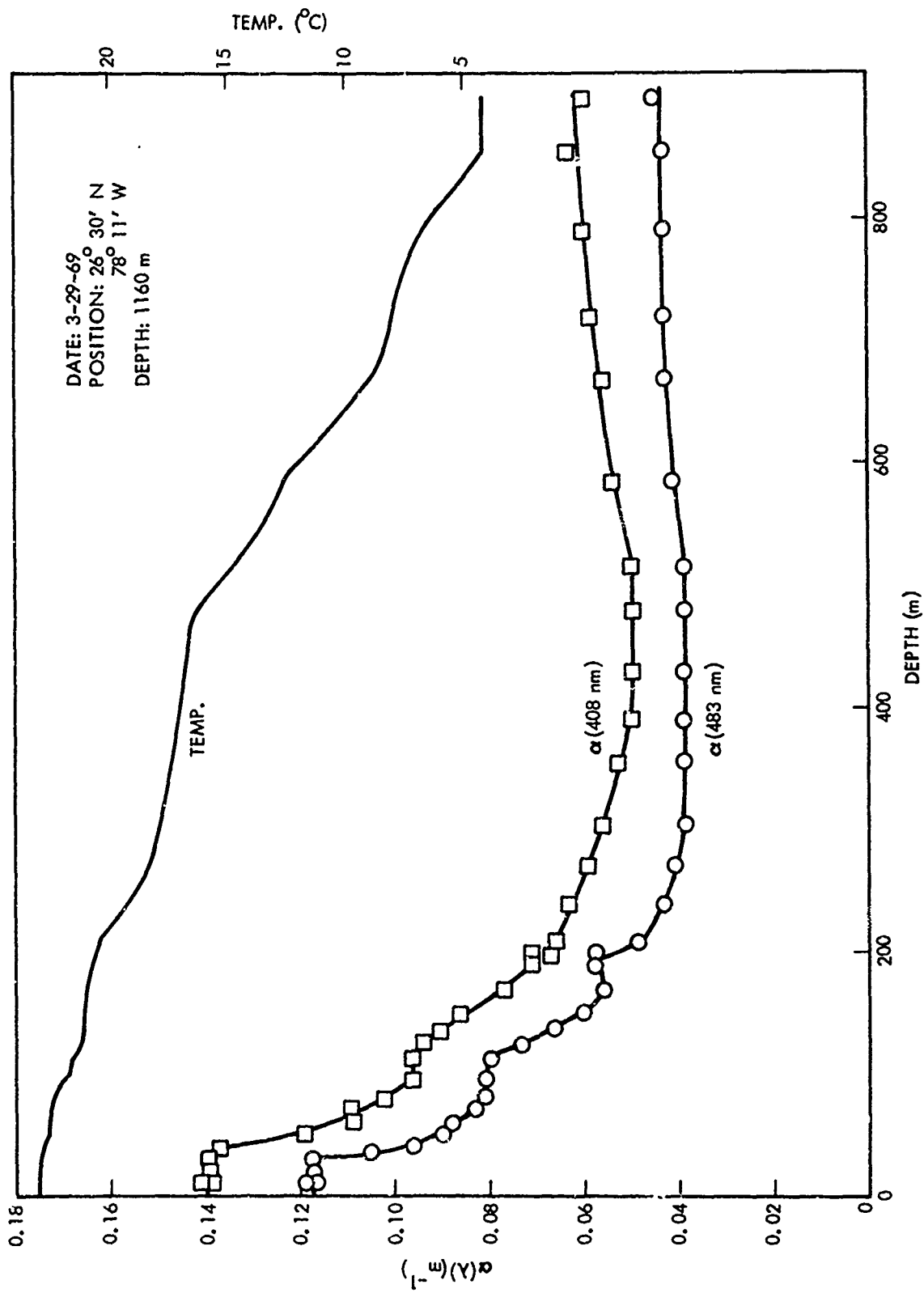


FIG. 3 OPTICAL ATTENUATION AND TEMPERATURE PROFILES OF DROP D-1

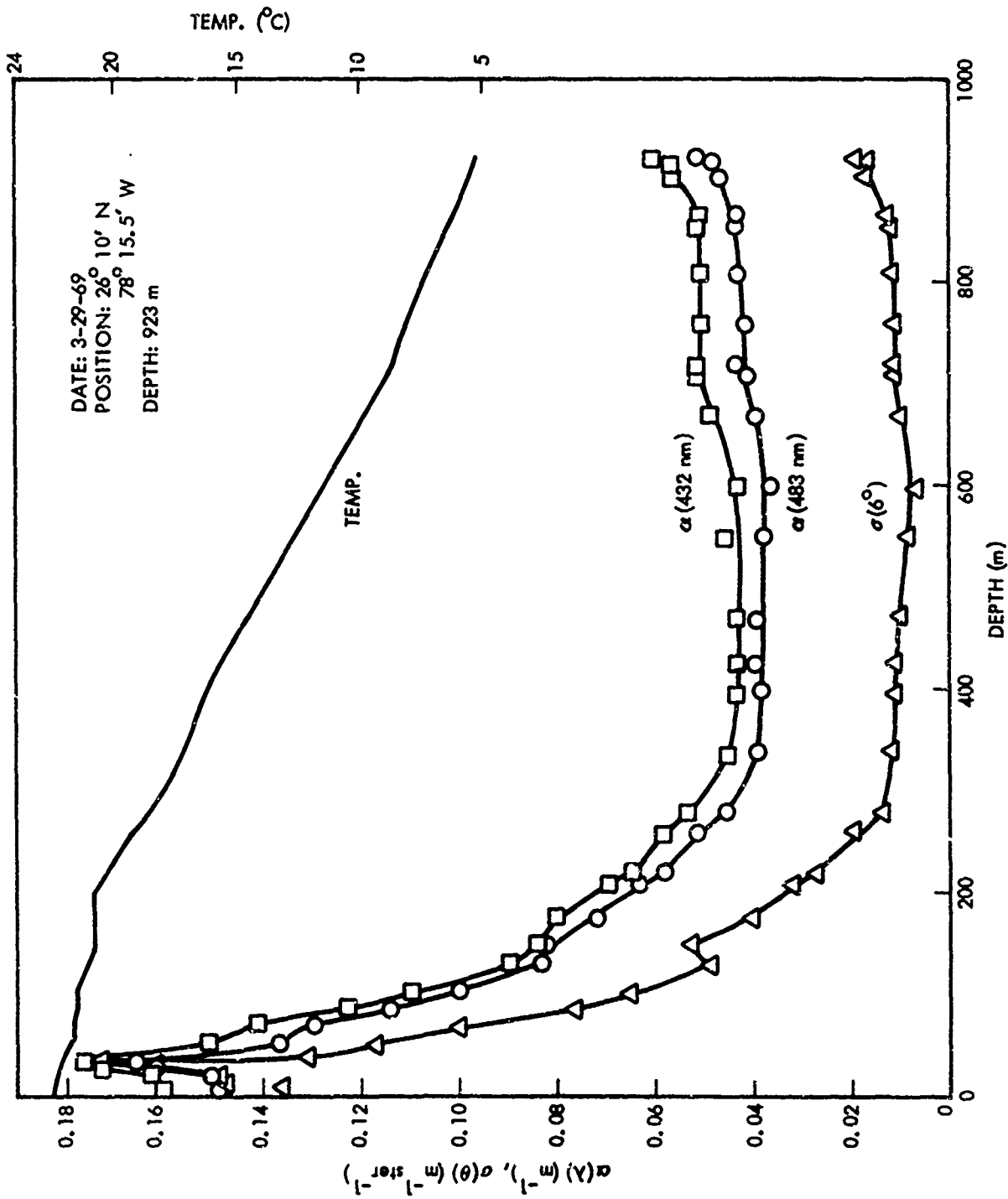


FIG. 4 OPTICAL ATTENUATION AND TEMPERATURE PROFILES OF DROP D-2

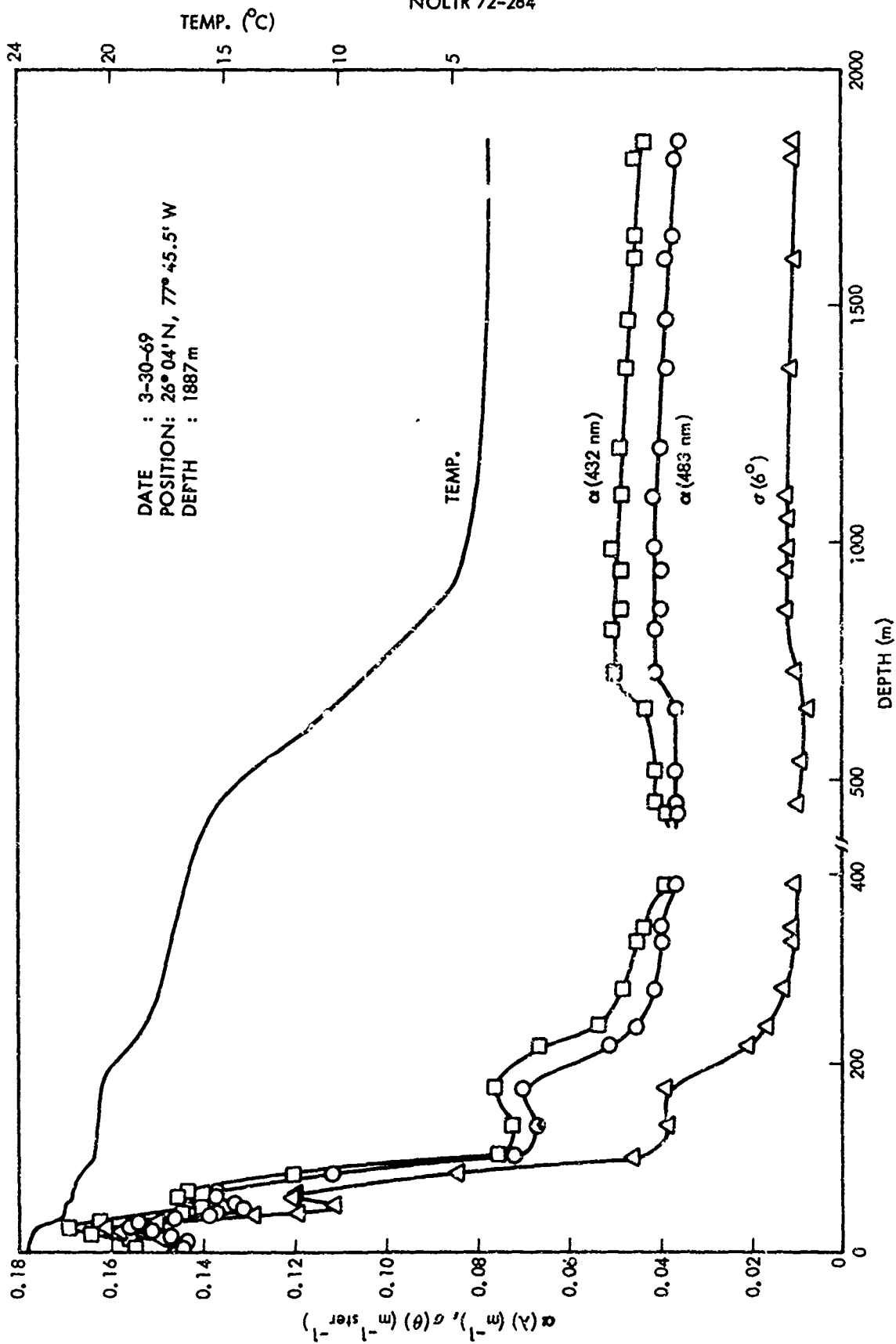


FIG. 5 OPTICAL ATTENUATION AND TEMPERATURE PROFILES OF DROP D-3

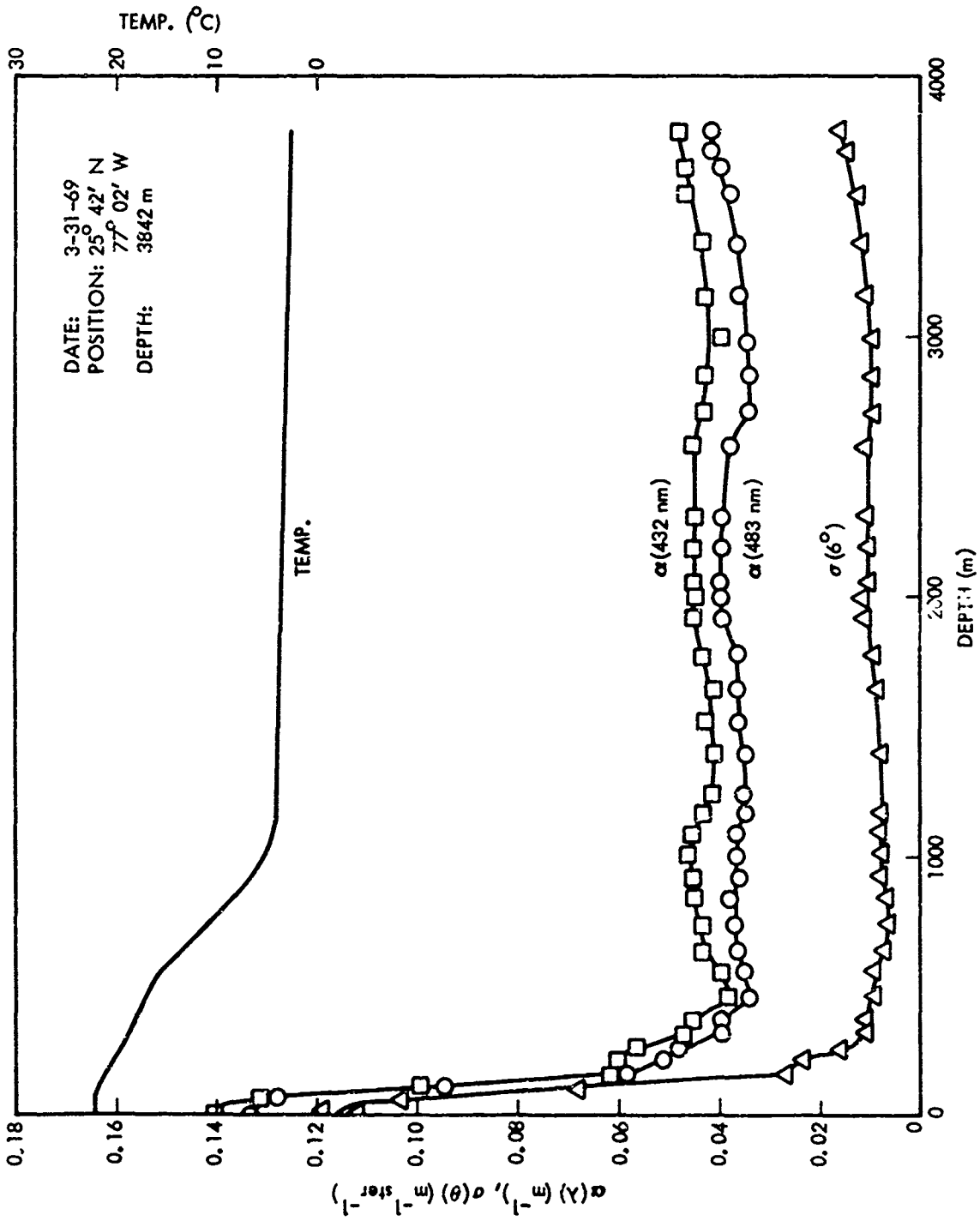


FIG. 6 OPTICAL ATTENUATION AND TEMPERATURE PROFILES OF DROP D-4

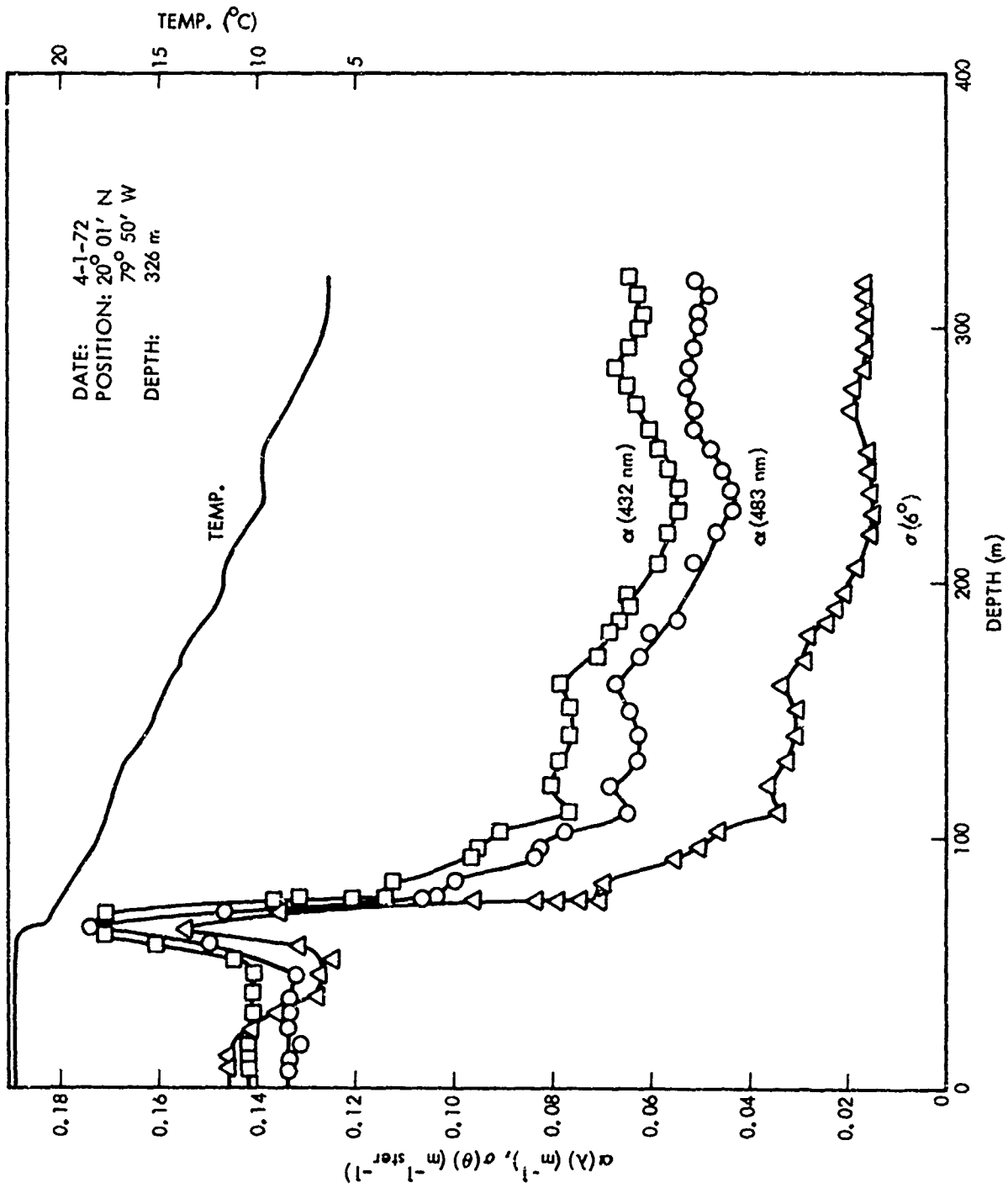


FIG. 7 OPTICAL ATTENUATION AND TEMPERATURE PROFILES OF DROP D-5A

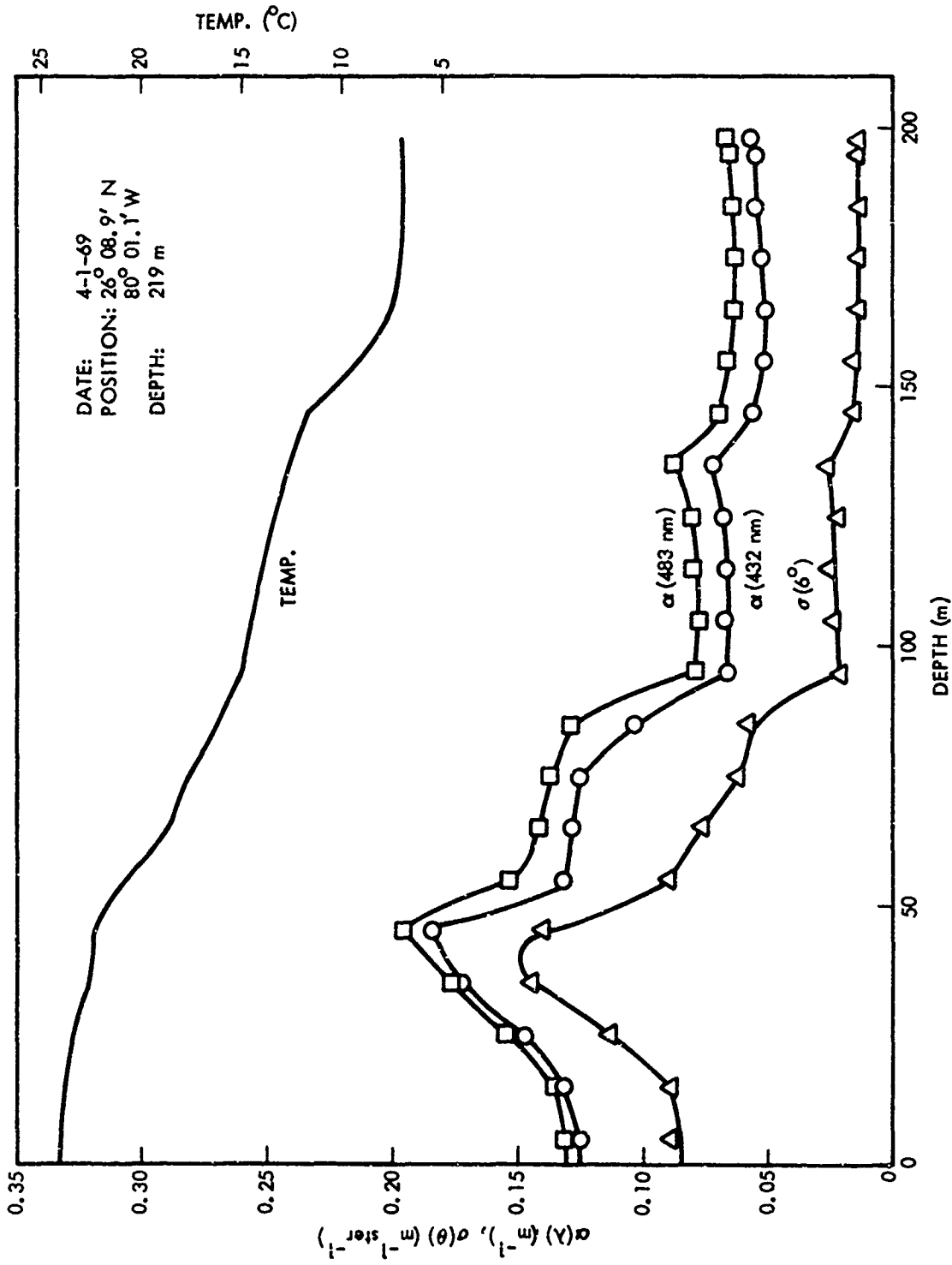


FIG. 8 OPTICAL ATTENUATION AND TEMPERATURE PROFILES OF DROP D-5B

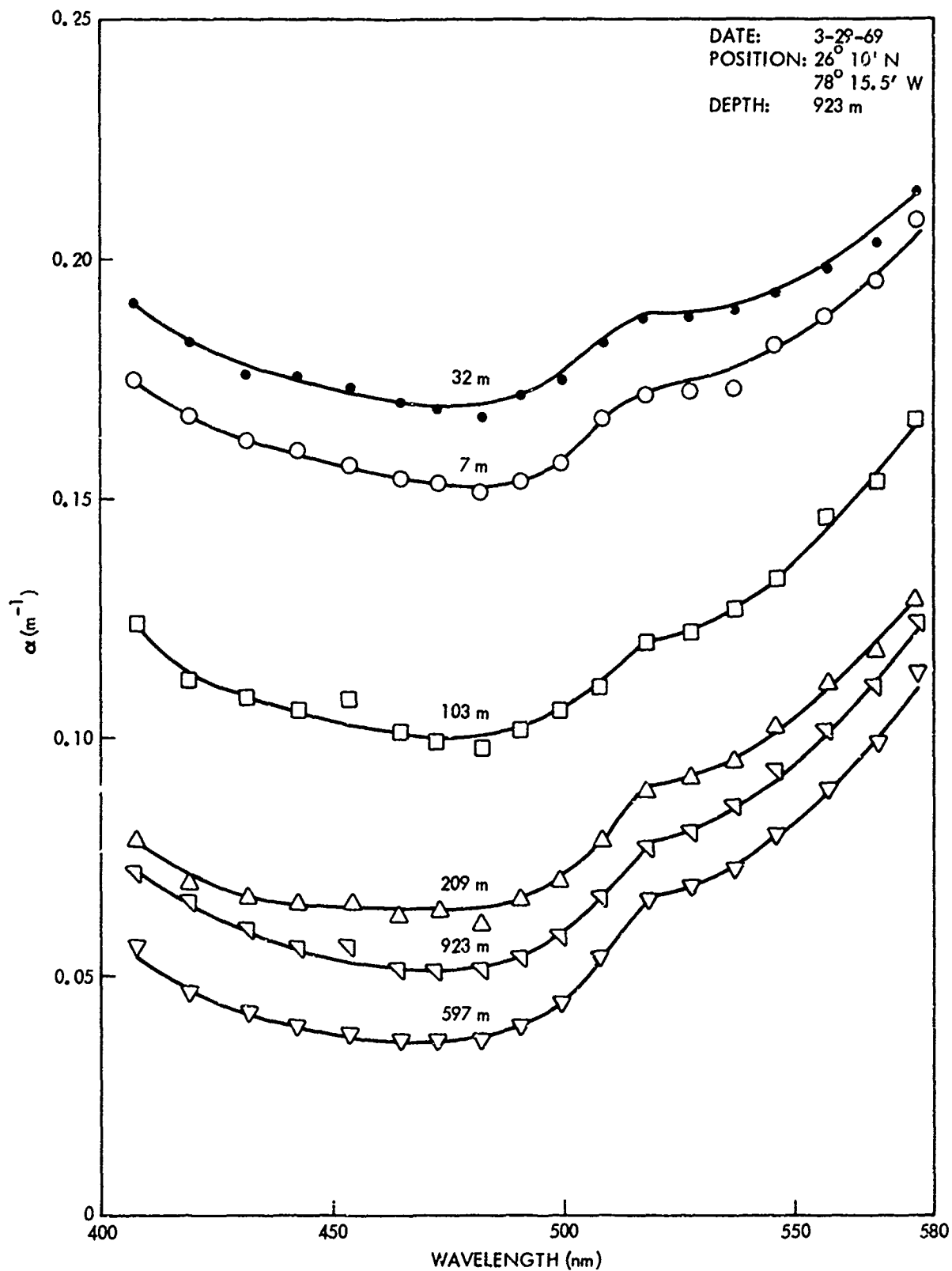


FIG. 9 OPTICAL ATTENUATION SPECTRA OF DROP D-2 AT SELECTED DEPTHS

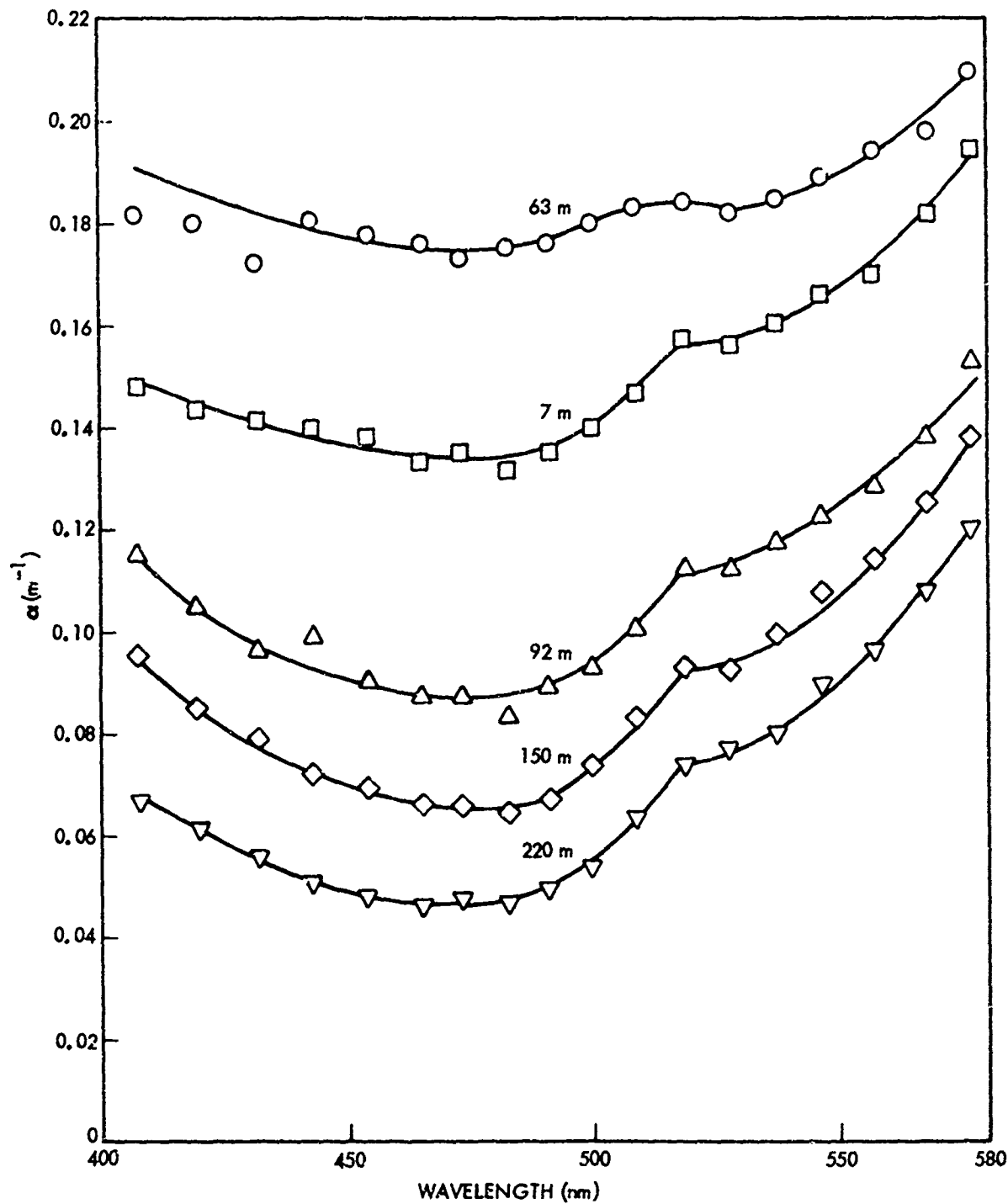


FIG. 10 OPTICAL ATTENUATION SPECTRA OF DROP D-5A AT SELECTED DEPTHS

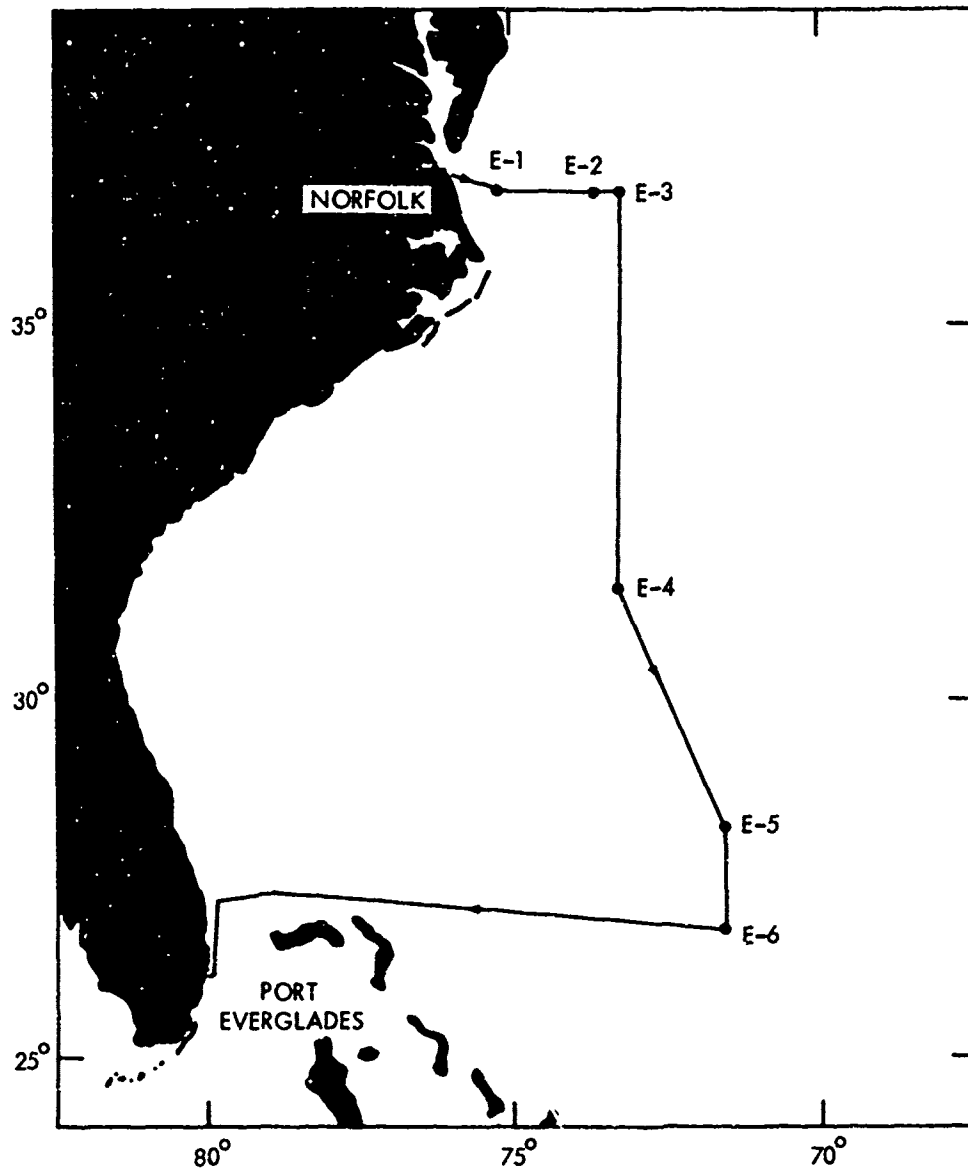


FIG. 11 TRACK CHART OF DOOM CRUISE E

44

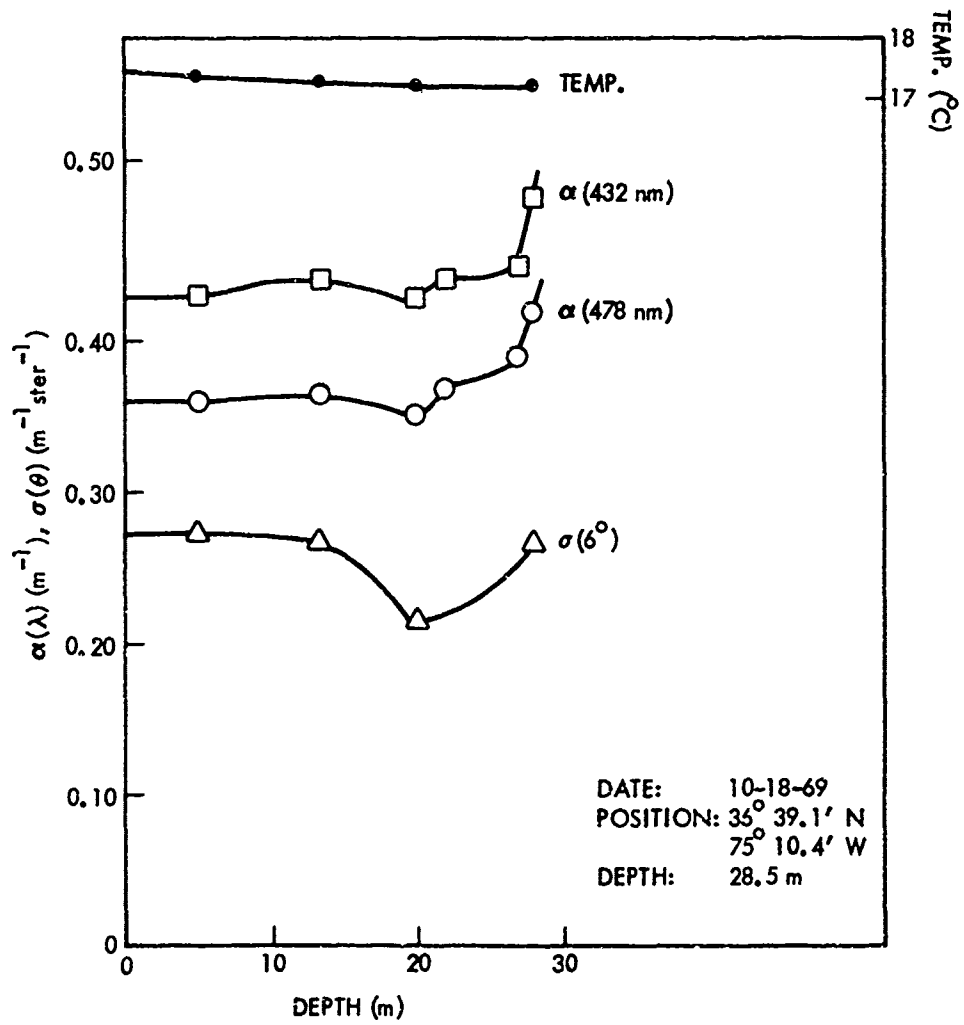


FIG. 12 OPTICAL ATTENUATION AND TEMPERATURE PROFILES OF DROP E-1

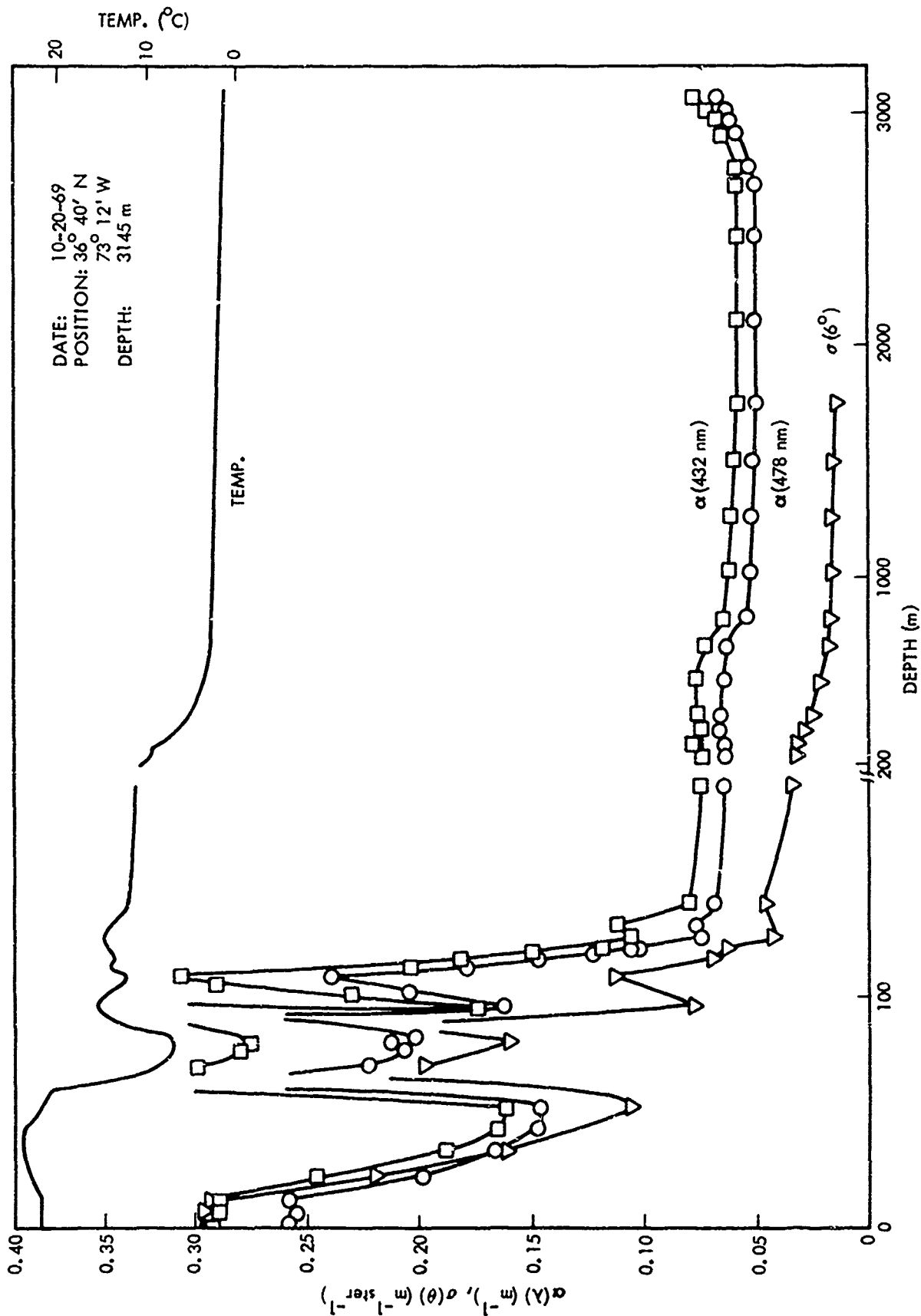


FIG. 13 OPTICAL ATTENUATION AND TEMPERATURE PROFILES OF DROP E-3

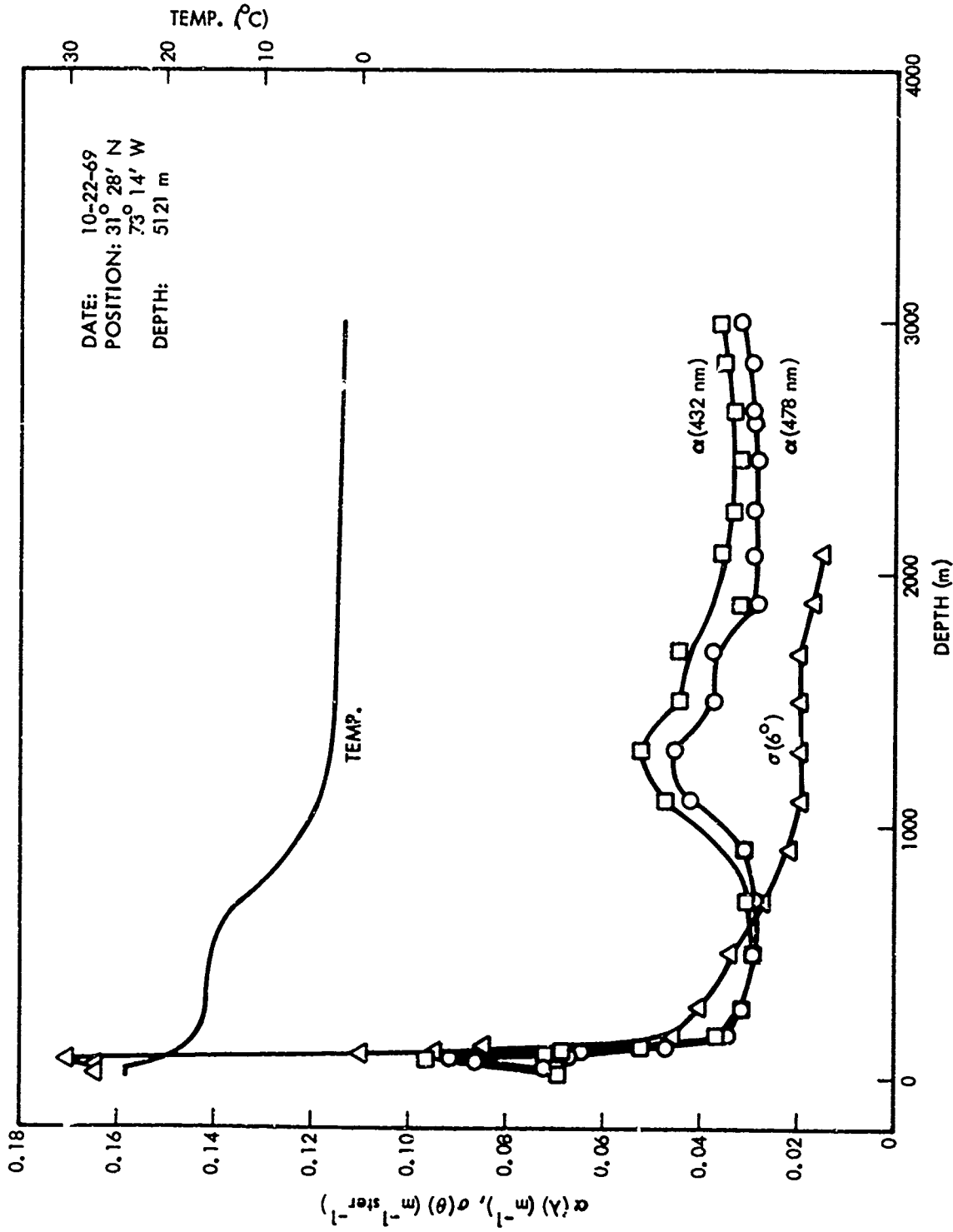


FIG. 14 OPTICAL ATTENUATION AND TEMPERATURE PROFILES OF DROP E-4

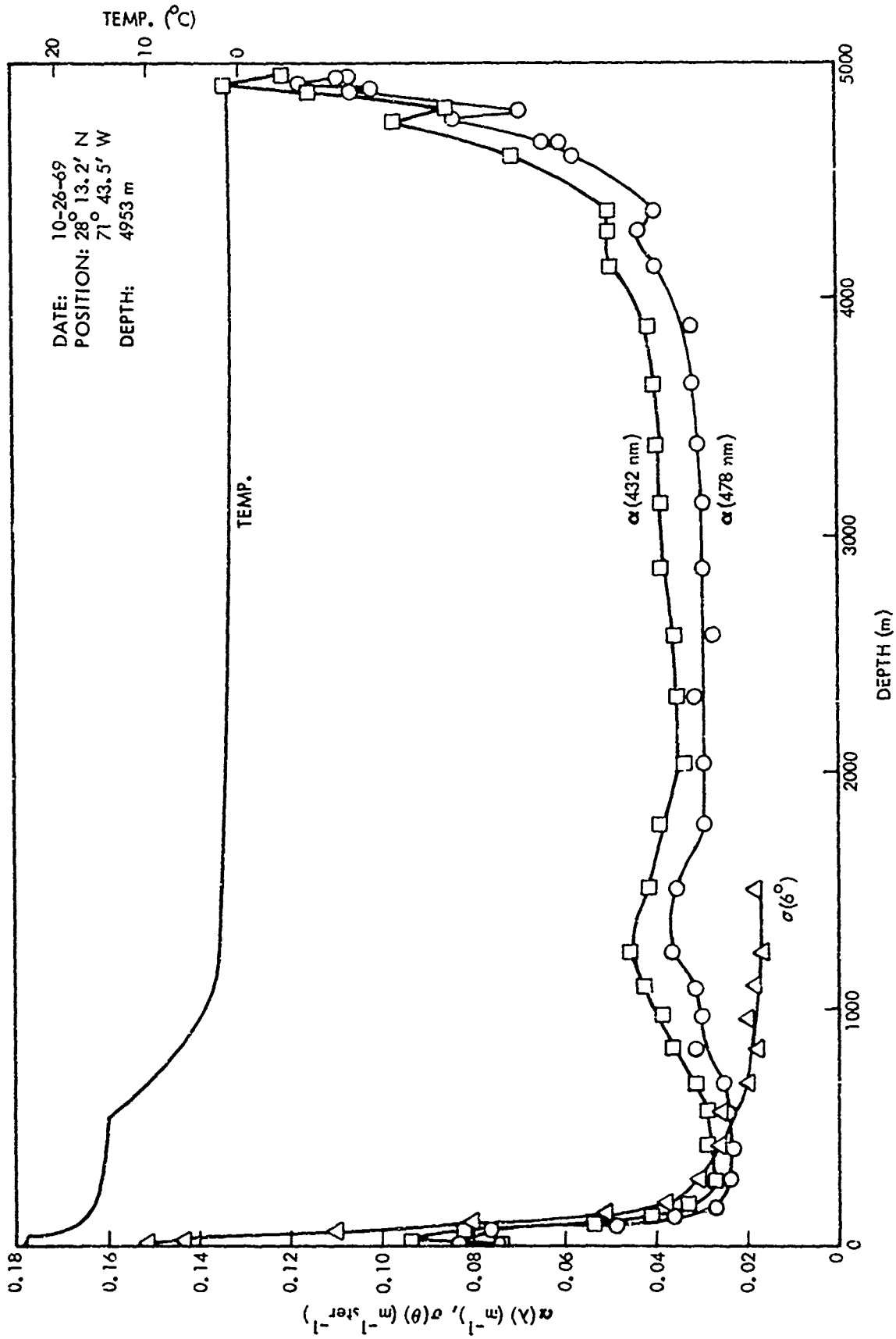


FIG. 15 OPTICAL ATTENUATION AND TEMPERATURE PROFILES OF DROP E-5

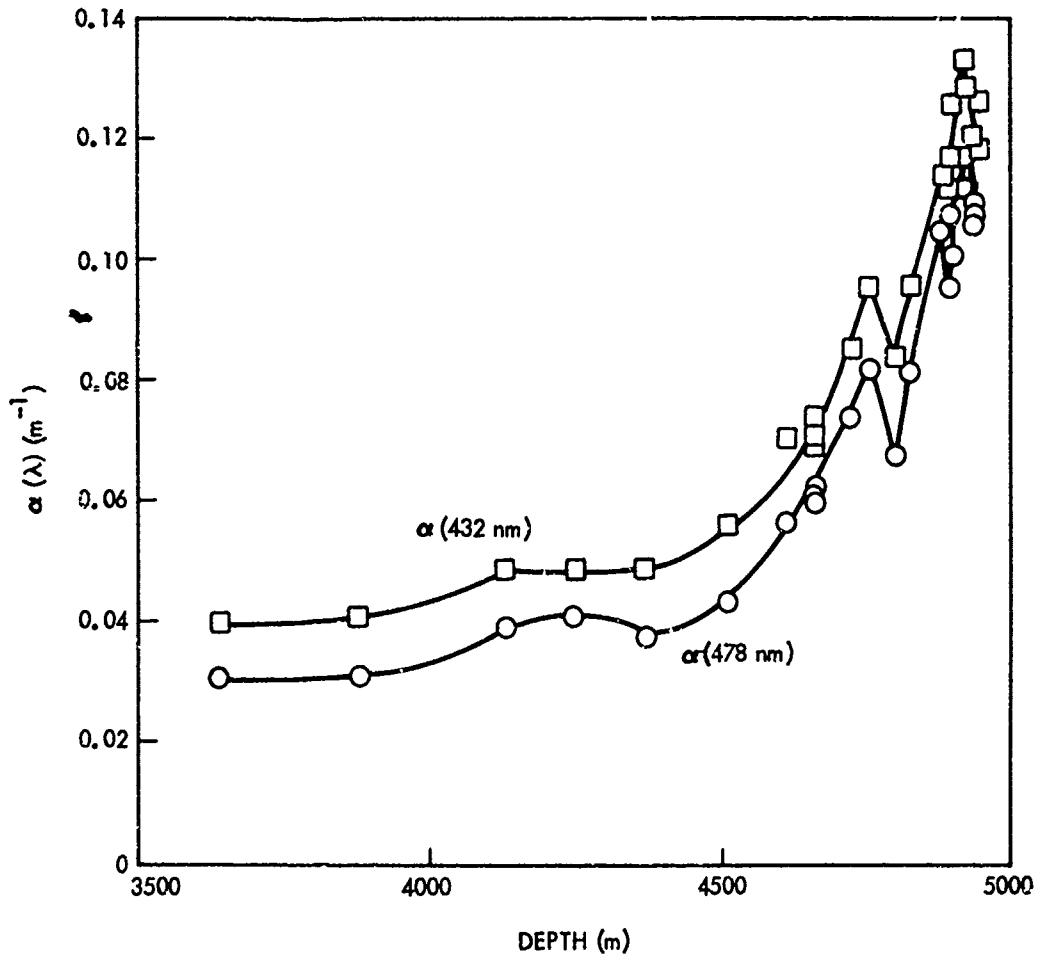


FIG. 16 OPTICAL ATTENUATION PROFILES OF BOTTOM WATERS OF DROP E-5

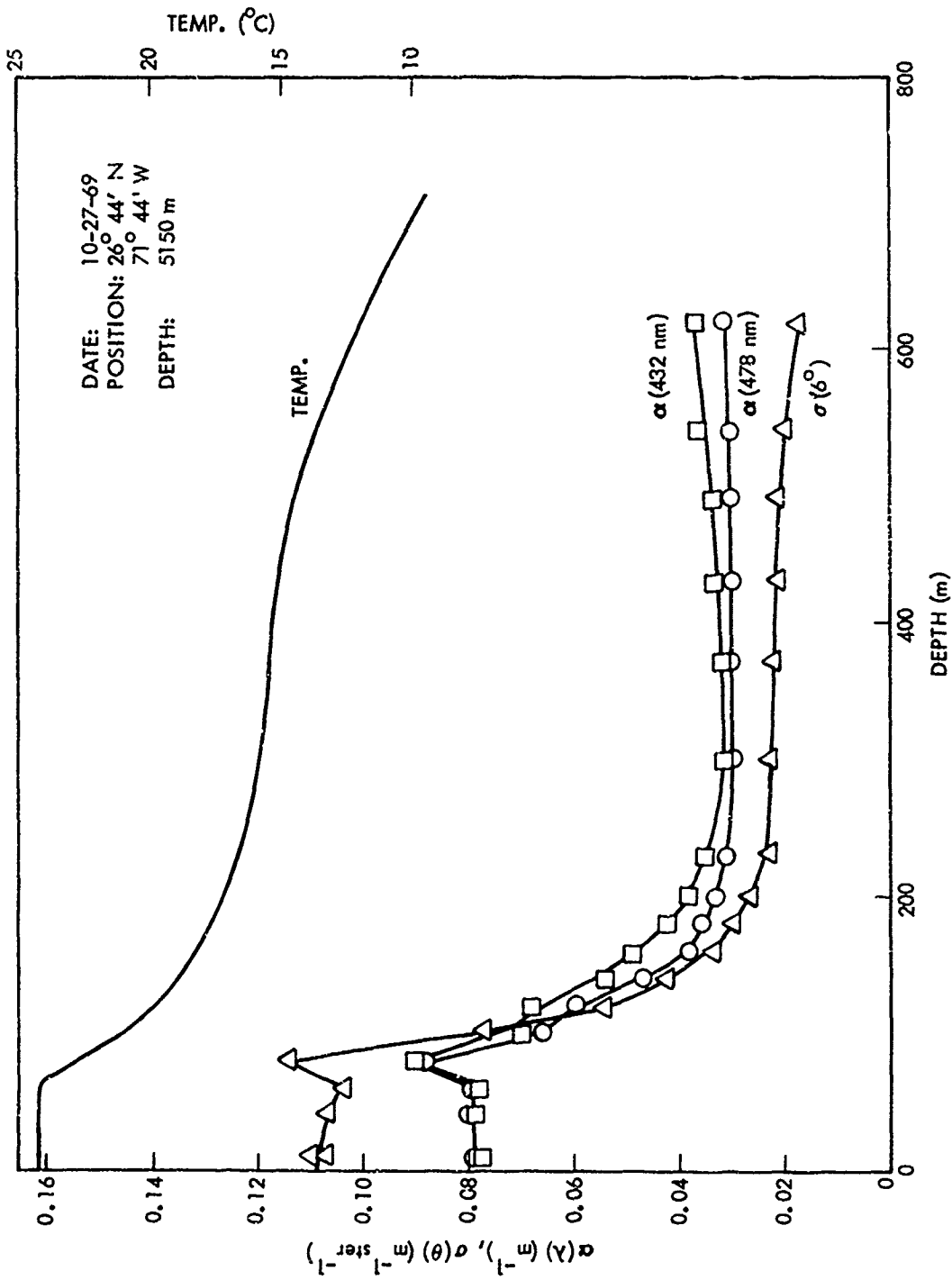


FIG. 17 OPTICAL ATTENUATION AND TEMPERATURE PROFILES OF DROP E-6

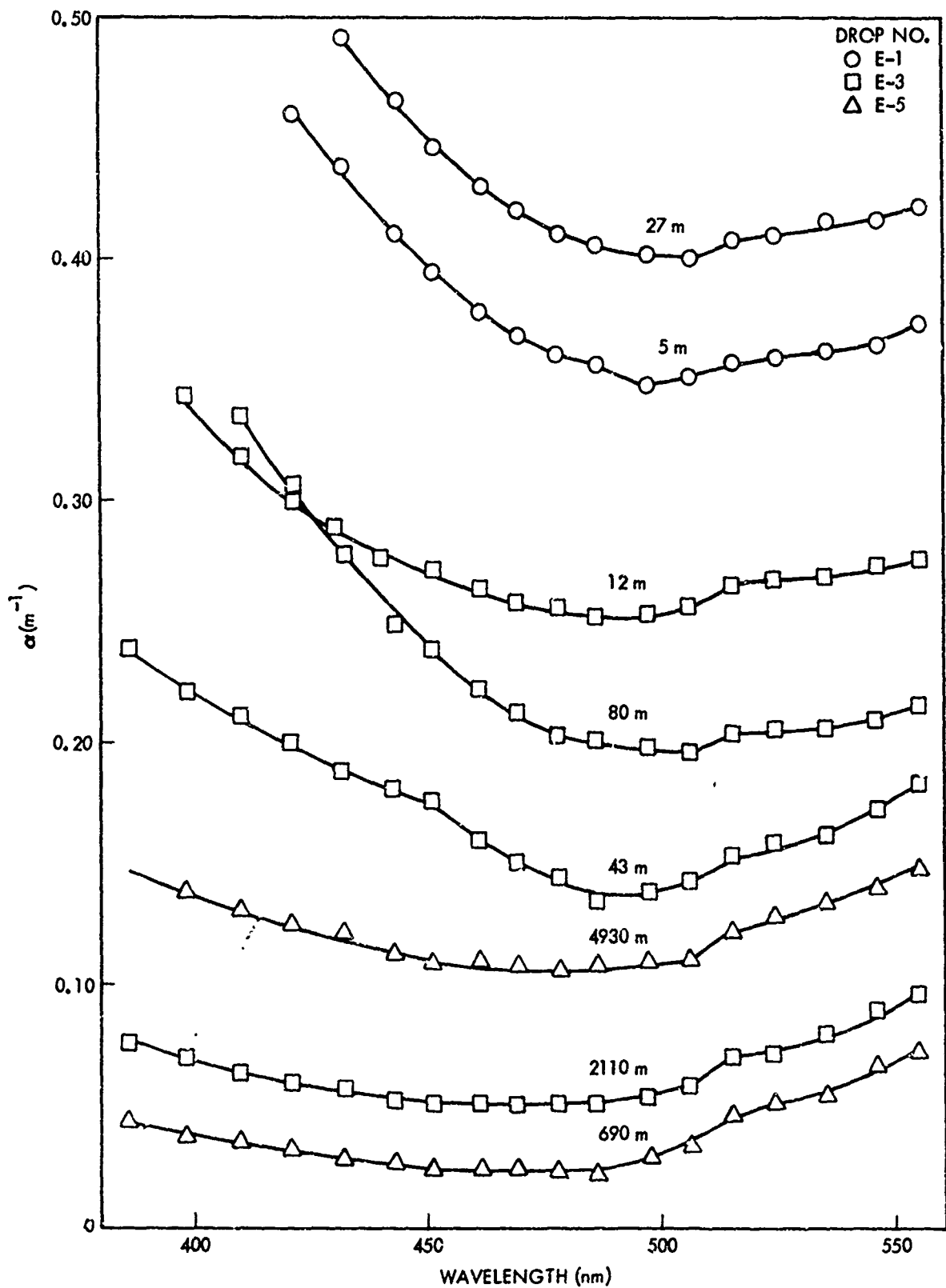


FIG. 18 COMPARATIVE ATTENUATION SPECTRA FROM THREE CRUISE E DROPS

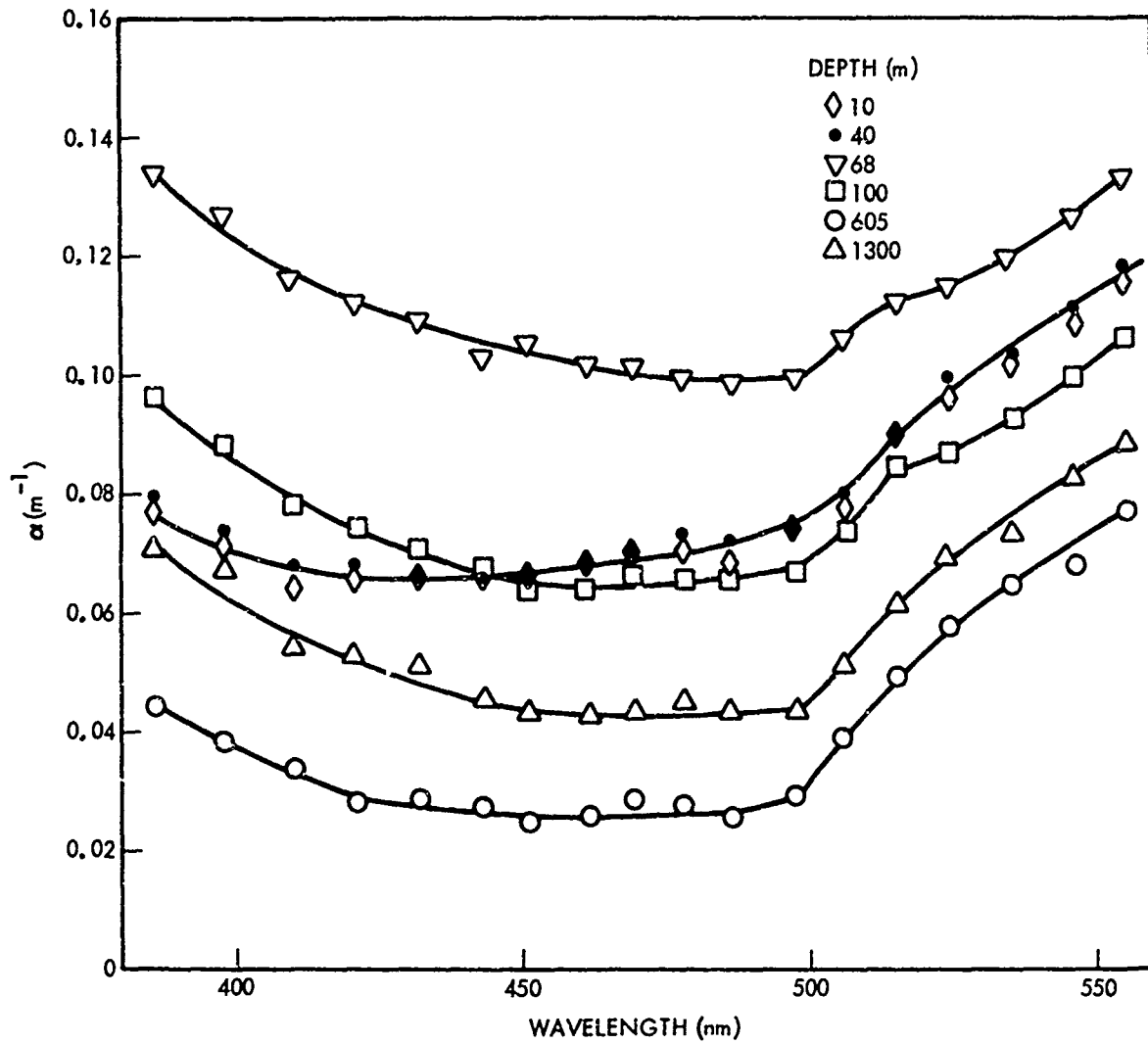


FIG. 19 OPTICAL ATTENUATION SPECTRA OF DROP E-4 AT SELECTED DEPTHS

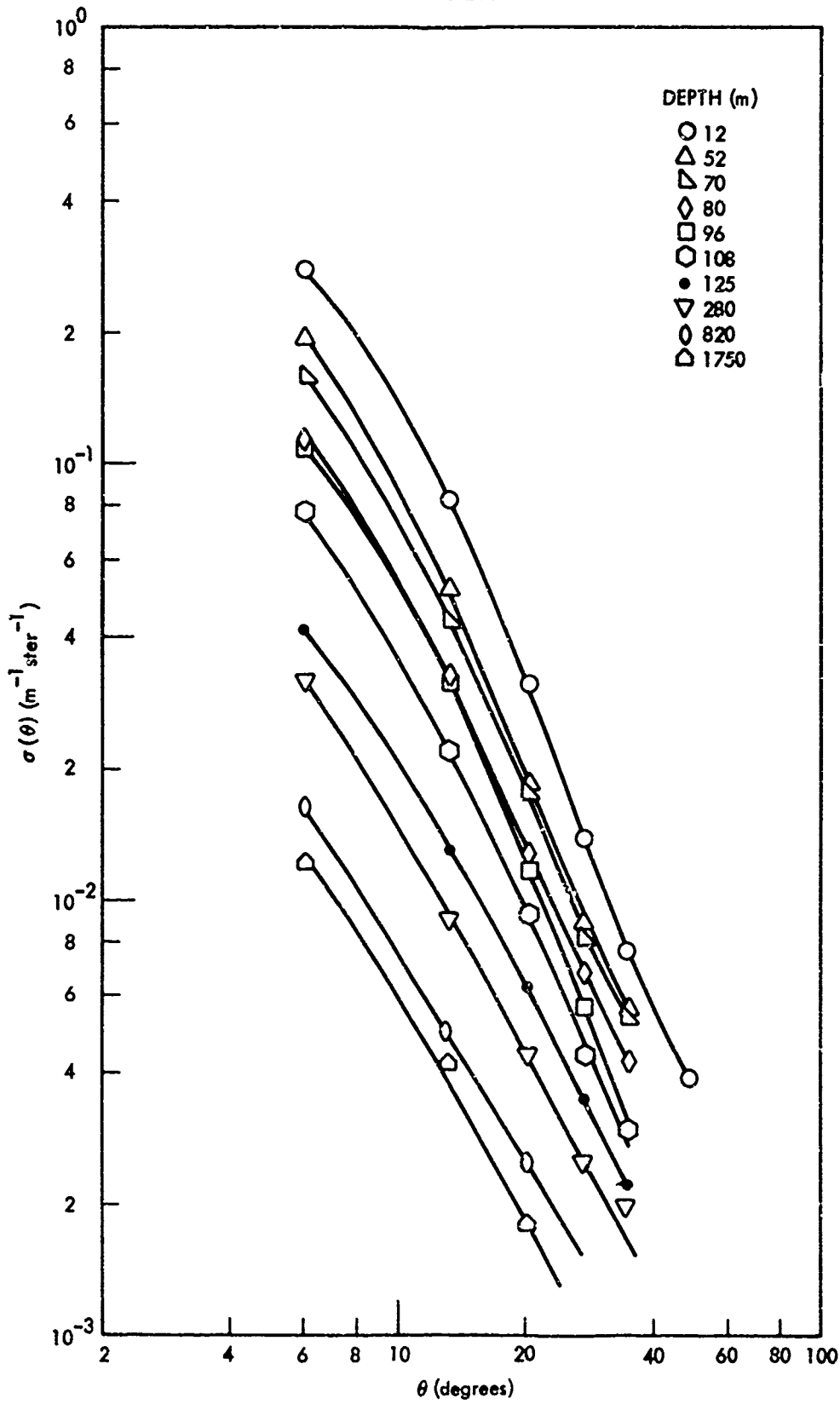


FIG. 20 VOLUME SCATTERING FUNCTIONS AT SELECTED DEPTHS FOR DROP E-3

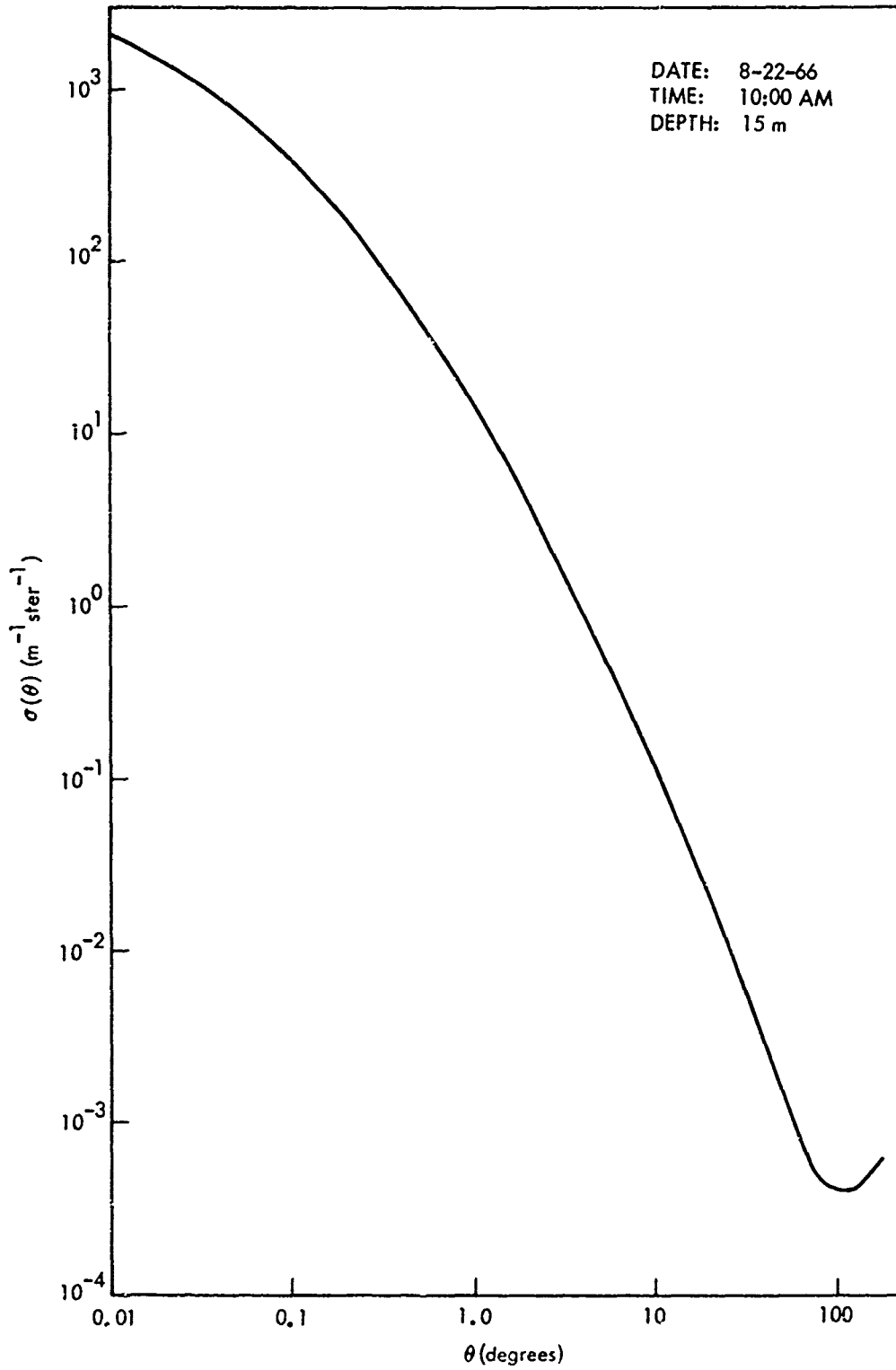


FIG. 21 VOLUME SCATTERING FUNCTION AS COMPUTED BY MORRISON FROM ARGUS ISLAND MEASUREMENTS

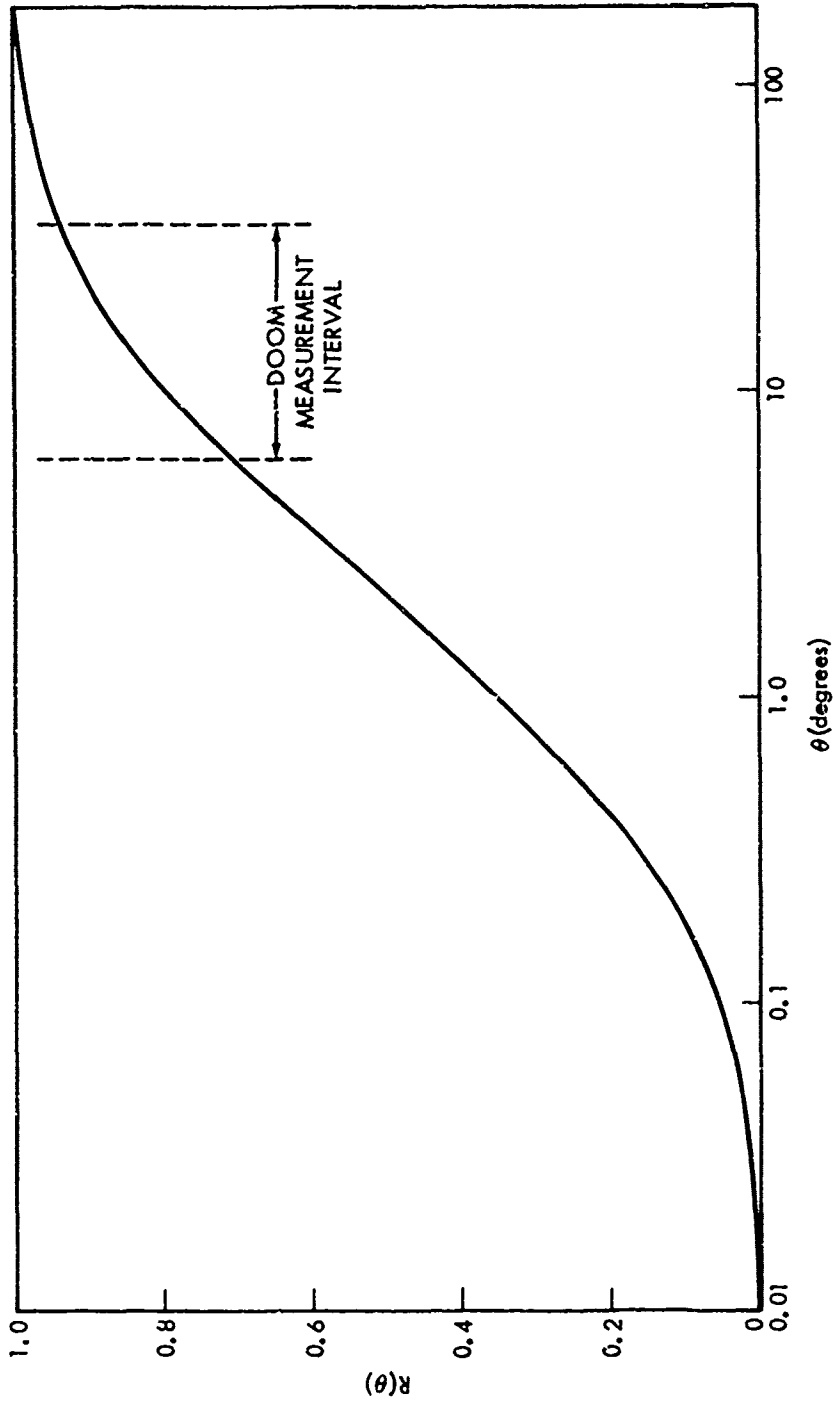


FIG. 22 $R(\theta)$ vs SCATTERING ANGLE FOR SELECTED SCATTERING DATA OF MORRISONS FROM ARGUS ISLAND DURING AUGUST 1966

APPENDIX

Two illustrations in the first printing of NOLTR 70-165 inadvertently included errors which may best be described as clerical or mechanical in nature. These figures, 17 and 22 of the original report were corrected for the second printing in early 1972 and are reproduced in the proper form as Figures A1 and A2 of this appendix. The error of Figure A1 was simply that of transposition of the wavelengths designating the two attenuation profile curves. In Figure A2 the curve of Hulbert's data was incorrectly copied for wavelengths above the transmission window from 460 to 580 nanometer wavelengths.

Some questions have arisen concerning the sample volume of the spectral attenuation measurement which basically is an 8-pass White optical system ^(R) which provides the 7.5 meter folded water path. These exterior optics are shown schematically in Figure A3 along with the conjugate source and receiver optical systems within the optics cylinder which serve respectively to project the source light into the water and then collect the remaining flux after traversal of the sample volume. The exit slit of the source monochrometer, S_E , is focussed by lens, L_1 , to form an image S_1' , beyond the exit window of the optics cylinder, W_1 , in the water at the entrance plane of the White optical system. The White system consists of three identical front surface spherical mirrors, M_1 , M_2 , and M_3 with radii of curvature of 910 millimeters and with free apertures of about 70 millimeter diameter. Mirrors are arranged as shown in Figure A3 with adjacent mirrors M_1 and M_3 separated from M_2 by a distance equal to the 910 millimeter radius of curvature. Since the center of curvature of mirrors M_1 and M_3 are located respectively at C_1 and C_3 upon the surface of M_2 , M_1 and M_3 serve to repeatedly re-image the initial exit slit image S_1' in a line from the entrance aperture of the White system at S_1' , across the face of mirror M_2 , to the exit plane of the system at S_5 . The center of curvature of M_2 is centrally positioned at C_2 between M_1 and M_3 and thus functions to image M_1 upon M_3 . In Figure A3 where the system is shown as adjusted for eight traversals of the incident light, the slit image S_1' is re-imaged by M_1 at S_2' . S_2' is imaged at S_3' by M_3 , S_3' is imaged at S_4' by M_1 , and finally S_4' is imaged by M_3 at S_5' coincident with the exit aperture of the White system. Minor adjustments of the positions of the center of curvature of M_1 and M_3 permit operation in a four pass mode. From S_5' light re-enters the optics cylinder and is imaged by lens L_2 at the entrance aperture A3 of the optical receiver.

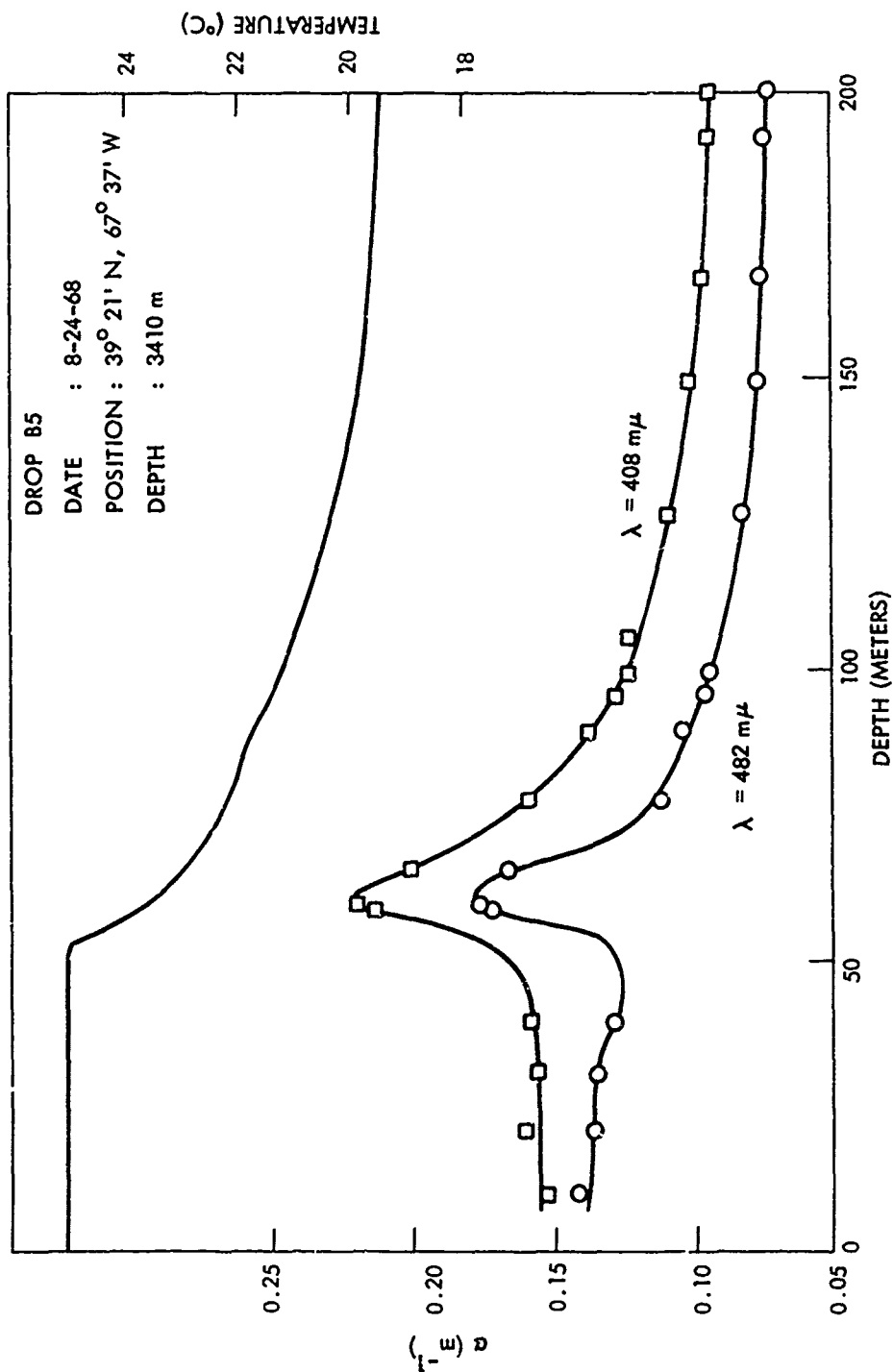
(R) John U. White, "Long Optical Paths of Large Aperture", J. Opt. Soc. Am., 32, 285 (1942)

The field stop A1 is imaged by the lens-window combination, L1 and W1, at the mirror M1. The exterior surface of W1 is ground with a slightly negative curvature very nearly equal to the radius of curvature of M1. Therefore the location of the image of A1 is essentially independent of the refractive index of the surrounding medium and thus remains at M1 for both the air calibration and in situ measurement cases. Size of the image however does vary, decreasing from a diameter of 44 millimeters in air to 33 millimeters in water. Window W2 similarly has a negative curvature so that the aperture A2 is always imaged at M3. Receiver apertures A2 and A3 are slightly larger than their counterparts on the source side in order to insure that the total flux bundle is passed to the detector.

Mirrors of the White system are front surface aluminum overcoated with a thin layer of silicon monoxide. The quality of the aluminum coating, that is, the absolute reflectivity of the mirrors, is not critical since the reflectivity terms in the calibration and in situ measurement equations cancel. What is of prime importance is the durability of the coating or the stability of the reflectivity as a function of exposure to the severe elements of the marine environment. This durability depends upon the quality of the SiO overcoat which functions solely to protect the aluminum coating. Perhaps erosion of the SiO by environmental elements may be a factor in mirror deterioration, but more likely, mirror degradation results from incomplete covering of the mirror surface in the form of small pinholes in the SiO coating. Upon exposure to salt water mirrors with the larger of these pinholes deteriorate quite rapidly and suffer major surface corrosion which is quite evident after but one short measurement drop. Fortunately such damage has occurred only rarely. More often deterioration is rather slow with a detectable loss in reflectivity requiring exposure to salt water and the marine atmosphere for a period of several days. These gradual reflectivity losses necessarily result in replacement of mirrors at sea at intervals varying from four days to a week. Conceivably this gradual deterioration could produce errors in data recorded during a drop since reflected light levels would drop as a function of time and consequently result in too large values of α . Data analysis has shown that this has not been a significant problem for the three hour interval of the DOOM measurement.

To eliminate problems associated with the aluminum mirror, we have switched to multi-layer dielectric coatings. At our request the Optical Coating Laboratory Inc. of Santa Rosa, California coated three of the DOOM spherical mirror blanks with an enhanced reflectivity coating in the blue-violet spectral region. Measured reflectivity was in excess of 99 percent at wavelengths from 380 to 550 nanometers. These test specimens were immersed in a circulating bath of artificial sea water for two periods totaling 70 hours and then subjected for 48 hours to a salt spray test, MIL-STD-202A, Method 101A. No visual deterioration or measured reduction in reflectivity was detected after these laboratory

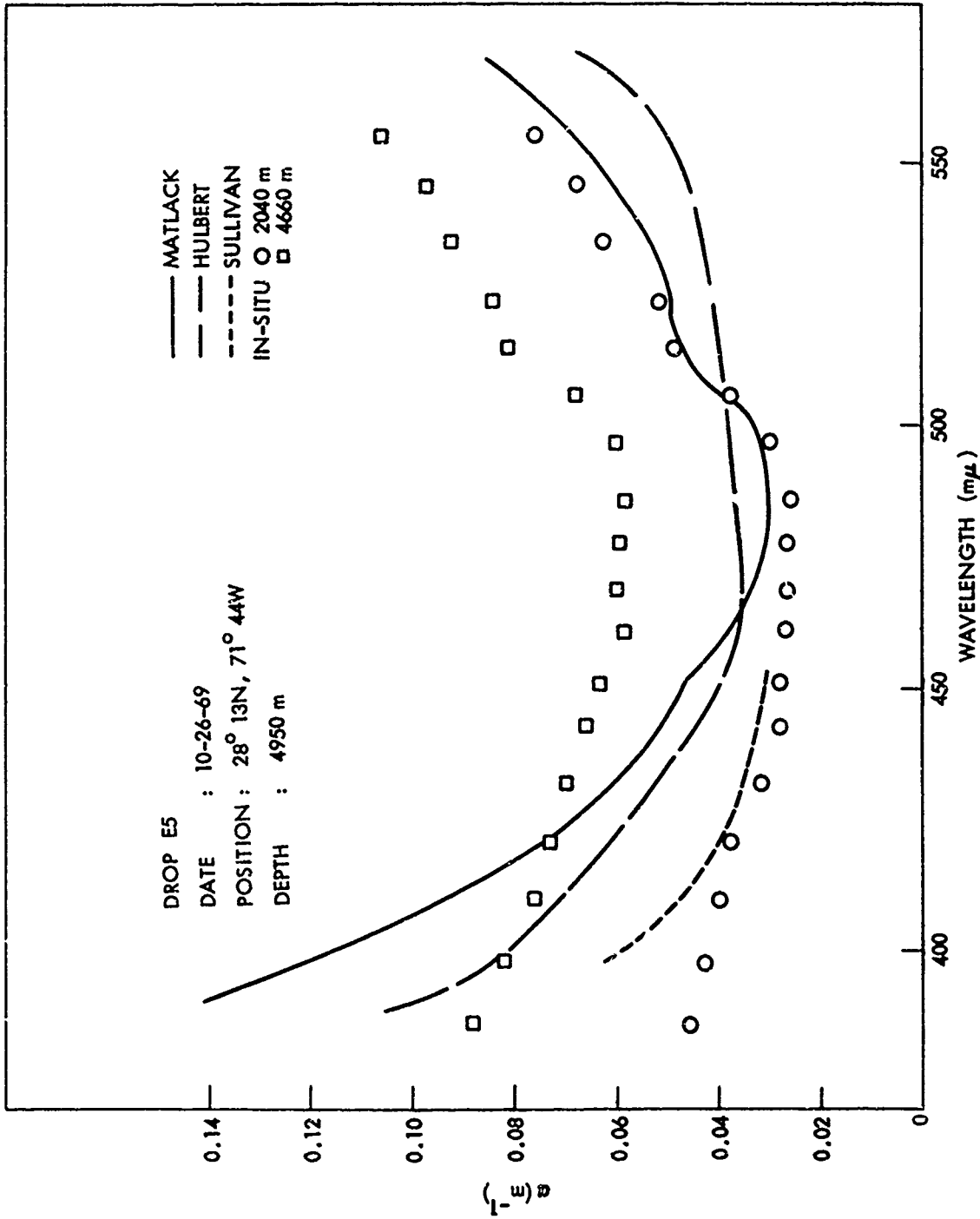
tests. These same mirrors were then installed in the DOOM instrument for subsequent operations in the Mediterranean Sea in the spring of 1972. During this 17 day cruise 13 measurement drops were completed. Submerged time totaled sixty hours. No visible damage to the mirror coatings was observed, nor was any significant drop in the signal level noted. Subsequent examination and measurement in the laboratory at NOL confirmed that the spectral reflectivity of the dielectric coatings had remained virtually unchanged over the duration of the cruise. The ability of the dielectric coatings to withstand the attack of corrosion within the marine environment was thus satisfactorily demonstrated at sea during the Mediterranean cruise.



OPTICAL ATTENUATION AND TEMPERATURE PROFILES OF SURFACE WATERS IN THE NORTH ATLANTIC

FIG. A1 CORRECTED FIG. 17 OF NOLTR 70-165

FIG. A1 CORRECTED FIG. 17 OF NOLTR 70-165



COMPARISON OF SPECTRAL ATTENUATION COEFFICIENTS OF PURE AND NATURAL WATERS

FIG. A2 CORRECTED FIG. 22 OF NOLTR 70-165

FIG. A2 CORRECTED FIG. 22 OF NOLTR 70-165

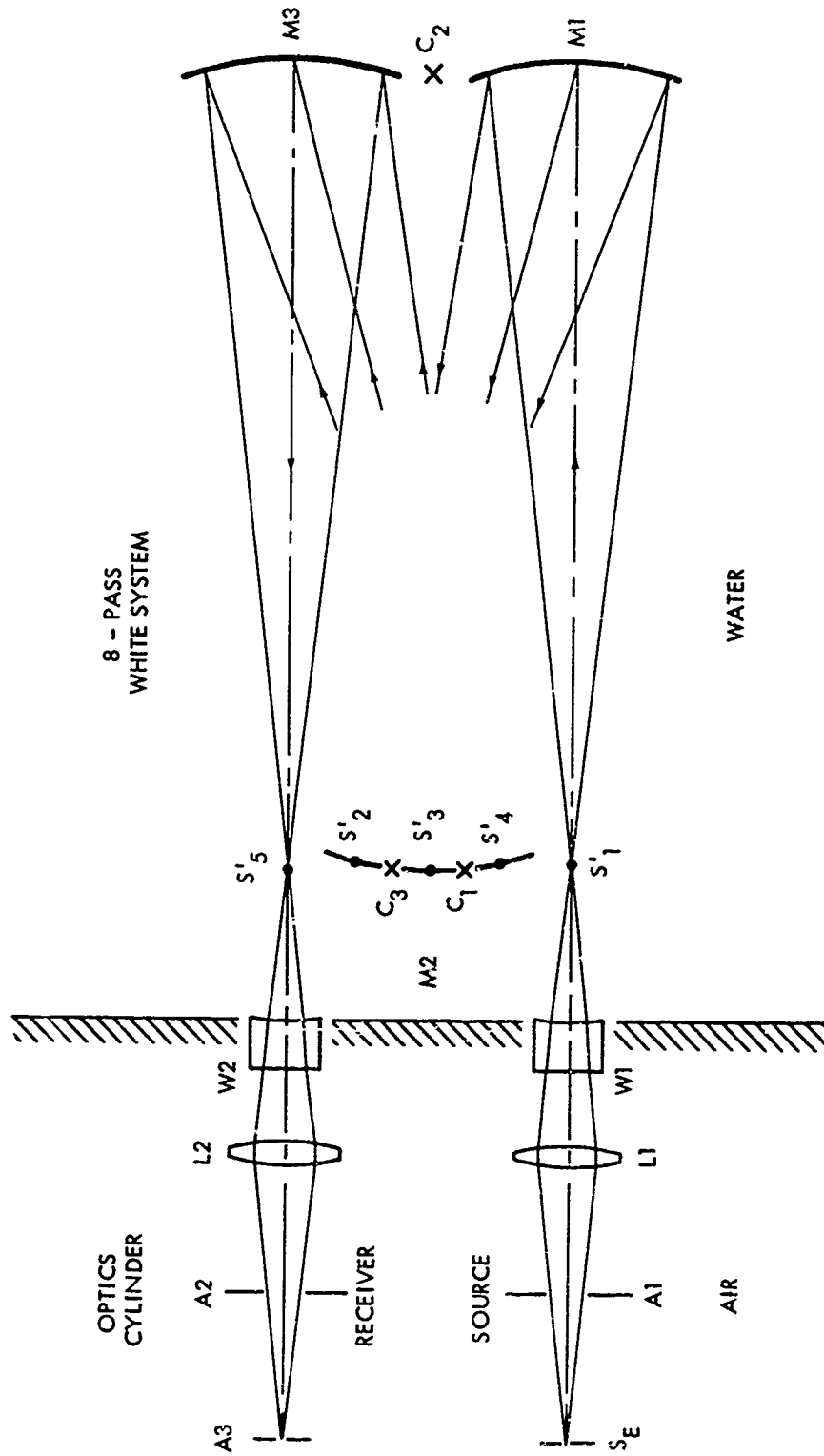


FIG. A3 SCHEMATIC OF THE EXTERIOR OPTICS OF THE ATTENUATION MEASUREMENT SECTION